

Metastable network phases from controlled self-assembly of high- χ block copolymersCheng-Yen Chang , Yun-Hao Chen , and Rong-Ming Ho ^{*}*Department of Chemical Engineering, National Tsing Hua University, Hsinchu 30013, Taiwan, Republic of China*

(Received 13 October 2023; accepted 1 February 2024; published 6 March 2024)

Well-ordered nanonetwork materials with triply periodic minimal surface texture are appealing and promising for innovative properties such as optical and mechanical metamaterials as inspired by nature (e.g., the photonic property from the wing structure of a butterfly and the high-impact property from the dactyl club of a mantis shrimp). Network structures possess self-supporting frameworks, open-cell character, high porosity, and large specific surface area, giving specific functions and complexity for practical applications. Here, a facile approach with simple routes for acquiring of metastable network phases beyond conventional phase diagrams is proposed and examined. By taking advantage of controlled self-assembly for high-interaction-parameter (χ) block copolymers (BCPs), it is feasible to acquire network phases from the use of a selective solvent for self-assembly under controlled evaporation of the solvent. In contrast with the thermodynamically stable equilibrium phases from intrinsic BCPs and their blends with conventional network phases, a variety of kinetically trapped network phases with a high degree of ordering can be obtained from a single-composition lamellar phase, giving an easy method to acquire metastable network phases even for a primitive phase with large packing frustration (i.e., entropic penalty). Furthermore, the windows for network phases can even be expanded through controlled self-assembly of star-BCPs as compared with the linear-conformation diblocks. As a result, the topological architecture of BCPs could be another controlling factor to vary the phase behaviors, which may provide easy access to a variety of metastable network phases from thermodynamically stable phases through a kinetically controlled process for self-assembly.

DOI: [10.1103/PhysRevMaterials.8.030301](https://doi.org/10.1103/PhysRevMaterials.8.030301)**I. INTRODUCTION**

Block copolymers (BCPs) with chemically distinct and incompatible blocks, which drive the assembly of molecule aggregates by both attractive and repulsive interactions, have diverse periodically ordered equilibrium states [1–3]. In the solution state with a solvent or diluent, the affinities of the constituted blocks in a BCP may create micellar morphologies with cylindrical, spherical, and laminated textures, even vesicles with simple contours or symmetries in local regions [4]. On the contrary, in highly concentrated BCP solutions, it is favorable to give a wide variety of self-assembled phases by tuning of effective volume fraction due to the swelling of the BCP with a solvent [5,6]. For self-assembly of BCPs in bulk, a variety of well-ordered phases such as spheres, cylinders, and lamellae as symmetrically labeled on common phase diagrams of BCPs can be formed [2,3]. As the rolling extension of research has expanded, more equilibrium phases have been studied in the past decades, including further classification of cylinders (tetragonally/hexagonally packing) and spheres (body-/face-centered packing) [7,8]. Apart from those

periodically ordering equilibrium with uniform curvatures, three-dimensional (3D) phases with complex texture, such as perforated lamellae and gyroid and orthorhombic networks, were discovered in neat BCP systems [9–18]. Indeed, there are more unusual phases showing unique structures involved with low-symmetric packings or even with a chiral sense obtained under specific requirements on chain conformations and/or segregation strength of the BCPs [16,19], which brings out opportunities for BCP self-assembly. As a result, it is feasible to acquire diverse ordered phases from the self-assembly of BCPs in solution and dried bulk state by controlling the phase behaviors thermodynamically and kinetically (see Fig. 1).

II. ORIGINS OF NETWORK PHASES: STABLE VS METASTABLE

In nature, network structures composed of colorless chitin make butterfly wings, beetle exoskeletons, and even bird feathers shine with dazzling colors [20–22]. The superior impact resistance on dactyl clubs of mantis shrimps originates from the bicontinuous network composites of hydroxyapatites and chitin, also true for starfish [23,24]. Getting to the bottom of nature, it is apparent that these examples share similar architectures, continuous and ordered networks, in common. Interestingly, the networks are the temporary results of evolution through billions of years since the appearance of organic creatures. The genuine biological crystals are generated from the creatures themselves and are usually involved with the self-assembly of amphiphilic

^{*}rmho@mx.nthu.edu.tw

Published by the American Physical Society under the terms of the [Creative Commons Attribution 4.0 International](https://creativecommons.org/licenses/by/4.0/) license. Further distribution of this work must maintain attribution to the author(s) and the published article's title, journal citation, and DOI.

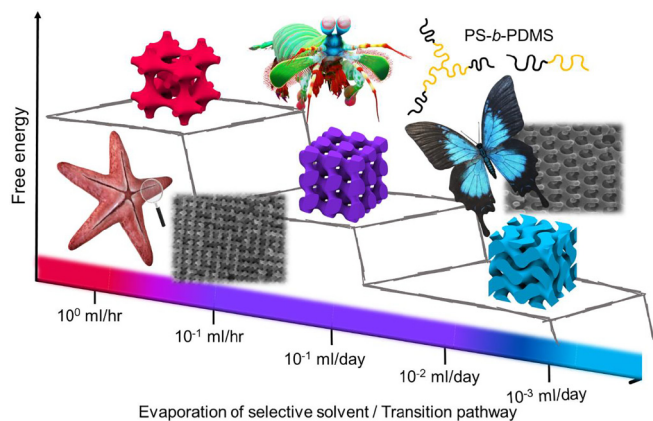


FIG. 1. Illustration of the controlled self-assembly for multiple network phases and the potential applications for biomimicking metamaterials.

supramolecules to give periodic structures [21,25]. In contrast to nature, well-ordered phases with triply periodic minimal surfaces (TPMSs) could be attained from the self-assembly of synthetic BCPs, and most of them are cubic phases [9,13,14,26,27]. According to the numbers of struts at the jointed junctions, they are commonly categorized into four classes: gyroid, diamond, primitive, and others.

A structure with curvatures displaying a Schoen G surface and three struts at a node is named a *gyroid* and contains both fourfold and threefold axes of symmetry [28–30]. Moreover, the twisting network shows certain handedness by a spirallike framework, resulting in special chiral sense as + or – according to the rotating and translating arrangement of the nodes on Wyckoff position 16*b* [18,31,32]. Thomas *et al.* [26] and Bates *et al.* [2] found access to acquire gyroids constituting the

same composition through self-assembly of BCPs. In contrast with the single network which exists in nature (I4₁32), the self-assembled gyroid phase contains two independent networks with opposite chirality (Ia3*d*), named a *double gyroid* (DG), due to the mean field of distribution of polymer chains [3,33,34]. Many reports have proven the equilibrium DG phase in the phase diagram of BCPs, yet routes toward the gyroid phase are highly limited in a narrow window [2,33,35]. To lower the enthalpy in each segregated microdomain, the connected chains are stretched to prevent the entanglement and develop the area minimization at the interface (i.e., intermaterial dividing surface). Generally, ideal models with constant mean curvatures (CMCs) show lower interfacial energy than those with constant mean thickness (CMT). However, the stretching polymer coils prefer curvatures with CMT to avoid the divergent packing of polymer coils in the local region [36], where coils overstretch at the cores yet compress at the struts in a gyroid. Consequently, the entropic penalty of coils poses packing frustration to the formation of complex phases. Matsen and Bates [37] concluded with the narrow window of the gyroid phase by calculation of the curvatures to corresponding structures constructed by the prediction of self-consistent field theory (SCFT). The deviations of the curvatures from the ideal models with CMC are calculated, reflecting the degree of entropic penalty to polymers in the self-assembled phases. As shown in Fig. 2(a), the corresponding average of the distribution of mean curvatures $\langle H \rangle$ and especially for the standard deviation of mean curvatures σ_H to each structure are provided, implying the degree of packing frustration of corresponding structures. Approaches, for instance, rigid conformations of polymers or strong segregation strength (i.e., high- χ BCP), are therefore suggested to alleviate the packing frustration.

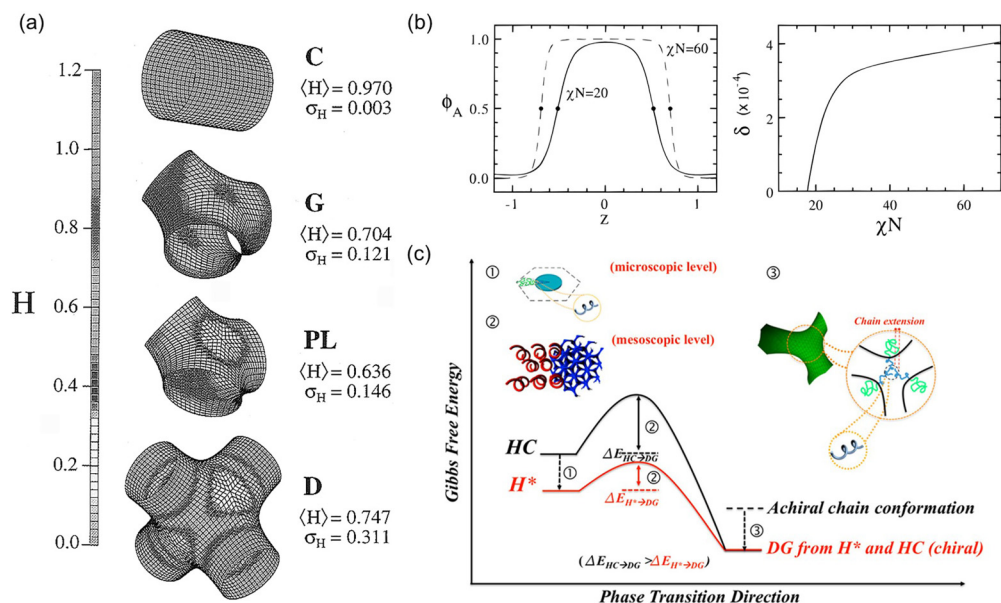


FIG. 2. (a) Interfacial surfaces corresponding to self-assembled phases of cylinder (C), gyroid (G), perforated lamellae (PL), and diamond (D) predicted by self-consistent field theory (SCFT). The calculated mean curvatures and standard deviations are provided [37]. (b) Cross-sectional profile of the composition in a microphase-separated microdomain and the deviation (δ) from the constant mean curvature (CMC) at different segregation strength [37]. (c) Illustration of suggested Gibbs free energy vs transition path to the formation of the double gyroid (DG) phase in chiral block copolymers (BCPs) with helical conformation in polymer chains [42].

Interestingly, in contrast with regular BCP systems with random coils, Ho *et al.* [16], Wen *et al.* [38], Wang *et al.* [39], Yang *et al.* [40], and Li *et al.* [41] introduced the chiral segments to one of the constituting blocks as chiral BCPs; chains with helical conformation would be formed due to the inter-chain interaction from the chiral molecules on the main chain. The chiral chains with helical conformation could effectively alleviate the packing frustration due to the unequal curvatures of the TPMS and therefore expand the possibility to reach the DG phase [Fig. 2(c)] [42]. Similar results were observed in the delicate synthesis with precise control of stereochemistry of monomers to design the tacticity of polymers, and beyond expectation, an unusual double network phase ($Pn\bar{3}m$) with more interconnecting struts can be captured [43,44]. A basic unit of the network displays four struts intersecting at a single node which locates at the diamond positions in a simple cubic lattice [30]. The presenting tetrahedral outlooks resemble a mathematically periodic surface, the Schwarz D surface, and is called the *diamond network* [45]. Contrary to the gyroid, the diamond network shows no chirality due to the missing inversion center. As mentioned above, the double diamond (DD) phase could be rarely found in self-assembly of BCPs with simple compositions, and that is mainly attributed to the fourth strut on the node; the additional one aggravates the issue of packing frustration of the complex structure resulting from the highly fluctuated curvatures at the nodes which requires stretching of polymers that can extend to the cores [Fig. 2(b)] [37]. As a result, the diamond phase is considered a metastable phase instead of an equilibrium phase plotted on conventional phase diagrams. To overcome the volume penalty from entropic constraints, minor components are added to fill the empty space. Blending of the homopolymers with the same composition as the minor components has been validated as an effective way to get the DD phase [46–48]. Introduction of third components can also assist the progress to overcome the entropic penalty, as demonstrated by Finnefrock *et al.* [49] and Han *et al.* [50]. The success of capturing the DD phase can be attributed to the smaller size of additives as compared with the long chains of BCPs that uniformly distribute over the whole microdomain. Additionally, the straightforward means of connecting a third component to the diblock polymer chains provides more extensive controllability to adjust the curving among the phase-separated microdomains [13,14,51,52]. A typical ternary phase diagram of tri-BCPs established by Epps *et al.* [13,14], Chen *et al.* [53], and Park *et al.* [54] demonstrates better opportunities to reach the equilibrium network phases, a core-shell DG and an alternating gyroid, where two networks randomly contain two different components. In recent years, Wang *et al.* [18] proposed that, by associating with chiral segments, the homochiral evolution from the molecular level realizes the concept of appointing the specific chirality to the single gyroid (SG) network; the achiral diamond networks were surprisingly obtained from the achiral form. The blending methods could be generally applied to obtain the DD phase via the cosurfactant effect [55,56]. As for the network with higher strut numbers, a class of networks different to the DG phase is also predicted as a metastable phase from self-assembled BCPs blends [47,48].

In the Schwarz surface family, a bulky branched framework with symmetry resembling the cubic primitive crystals

($Pm\bar{3}m$) is described, the Schwarz P surface, showing an orthogonal intersecting node with six struts; the periodic surface constructed a base-centered cubic lattice with hexapod nodes at the center sites [30,45]. In comparison with the gyroid and diamond, the double numbers of struts could result in a gigantic node size, enhancing enormous stress concentrated in the cores [47]; that reasonably explains the existence of the primitive network that can be found in nature but rarely from the self-assembly of supramolecules or BCPs [57]. The ultra-high packing frustration of the primitive network shows weak thermodynamic stability, making it a metastable structure the same as diamonds [37,47,58]. Similarly, the mean field regulates the formation of the primitive network phase to be double networks. The double primitive (DP) networks ($Im\bar{3}m$) was found in supramolecules/water mixtures, a biomimicking surrounding, where the aqueous solvent fills up the central regions of the micelles, avoiding the collapse of the bilayer membranes during assembly [59,60]; such a network phase can also be found in liquid crystals [61,62]. On the contrary, no report has been revealed for the discovery of the DP phase through the self-assembly of neat BCPs except for the BCPs/inorganic hybrids. Broadly speaking, most of them still appeared minor which could hardly be isolated from the majority of ordered phases [63].

As mentioned above, the triply periodic network phases are mostly in cubic lattices, including a I-WP network which resembles the wrapped package of interconnecting spheres [30,45,64,65]. The fourfold rotations of the octahedral basic units from bundles of four sticks lift to the genus surface as higher rotations to 12, and the puncturing spheres branch to eight neighboring punctured spheres in the space group of $Im\bar{3}m$. The I-WP network is more symmetric than it visually appears, yet it has been found in the exoskeleton of a longhorn beetle but never seen from self-assembled BCPs [65]. In comparison with the I-WP network, a simpler outlook of a network with three branches in orthorhombic lattice $fddd$ (O [66]) was predicted in self-assembled BCPs by SCFT and later on validated as an equilibrium phase near the windows of a DG phase [15,67]. Different to the observed network phases mentioned above, $fddd$ turns out to be the only single network phase with contours like a gyroid, but no helicity can be sensed [12]. The anisotropic extension/compression of branches in 3D breaks the volumetric symmetry so that it is excluded from the family of TPMSs. In general, approaches have been proposed to access the windows of most network phases in nature, including the control of stereochemistry or architecture of polymers and physical blending with polymers or inorganic solvents. The core issues are always about the precise control of compositions and how to alleviate the packing frustrations of the corresponding networks. In the following sections, we will discuss the alternatives to capturing network phases by a combination of thermodynamics and kinetics to adjust the progress of self-assembly of BCPs in a physical way.

III. COMPOSITIONAL CONTROL FOR SELF-ASSEMBLY OF BCPS

In the past decades, multiple approaches have been examined and demonstrated the accessibility to network phases in self-assembled BCPs. The compositional asymmetry

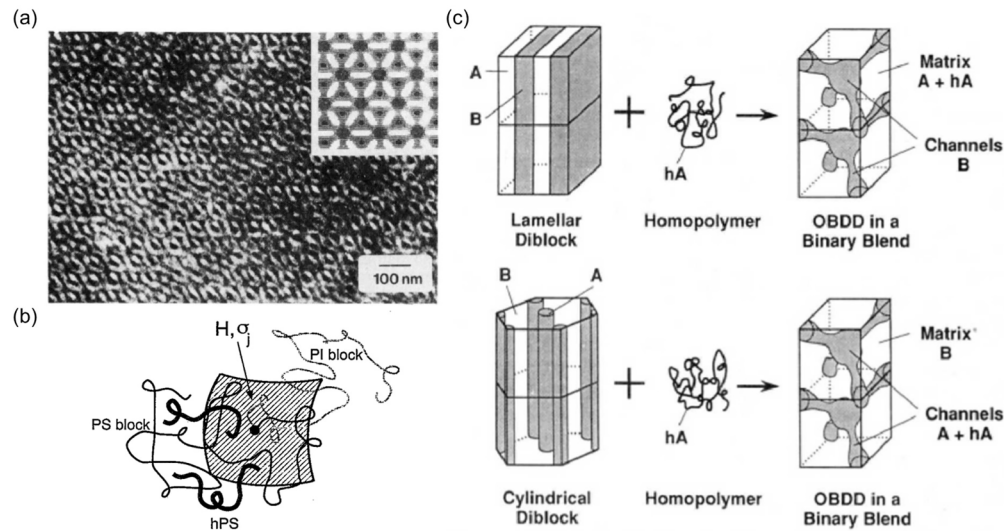


FIG. 3. (a) Transmission electron microscopy (TEM) micrograph of the self-assembled polystyrene-*block*-polyisoprene (PS-*b*-PB) blends with polystyrene (PS) homopolymer [73]. (b) Illustration of intermaterial dividing surface separating the PS and polyisoprene (PI) microdomain. The surface is characterized by interfacial mean curvature and average area per copolymer junction [74]. (c) Illustration of the formation of ordered bicontinuous double diamond from a lamellae-forming (top) and cylinder-forming (down) diblock copolymer and homopolymer [73].

naturally gives spontaneous curvature toward the part with minor volume [68]. A more complicated situation could be found in the BCP blends where the introduction of homopolymers could be served as dry or wet brushes dependent upon the relative chain length to the hosts [69,70]. The main issues of the approaches focus on the creation of the spontaneous curvature in self-assembled mesoatoms and distributions of building blocks in each microdomain to overcome the entropic penalty in complex network phases. Interestingly, the diverse ways for packing of polymer chains can create fascinating phase behaviors that enrich the traditional phase diagram of common di-BCPs. In the following sections, we include the accessibly approaches to the formation of network phases by BCP blends, precise design of multi-BCPs, and the spontaneous phase separation during the synthesis (i.e., polymerization-induced phase separation).

A. BCP blends

For the mixtures of BCP blends, the association of the additives with the BCP hosts can enrich the phase behaviors. Usually, the added ones are called *brushes*. Note that the types of additives are crucial to the final outcomes. Interpretation between a polymer brush and mobile polymer chains is categorized by the concepts of a *wet brush* (a swollen brush) or a *dry brush* (an unswollen brush). The most important factor to determine the behaviors of the brushes is the relative chain lengths of the brushes to the hosts. For instance, for a binary mixture of di-BCPs (A-B) and homopolymers (A), the factor (α) is defined by the ratio of the degrees of polymerization in the mixture. Here, $\alpha = N_{A,h}/N_{A,c}$, where $N_{A,h}$ and $N_{A,c}$ correspond to the homopolymers and BCPs, respectively. When $\alpha \geq 1$, the macrophase of the brushes and hosts may occur. The sizes of the A blocks remain without swelling. On the contrary, when $\alpha < 1$, the homopolymers are uniformly distributed in the A microdomains

(uniform solubilization), resulting in the swelling of the A blocks and an increase of the interfacial areas. The addition of the homopolymers may alter the interfacial curvature, as the loss of entropic penalty is compensated [70–72]. Especially for the network phases with TPMSs, the inconsistent curvatures lead to greater loss of entropic penalty. Winey *et al.* [73] demonstrated the access to acquire the DD phase in common AB-type diblock polystyrene-*block*-polyisoprene (PS-*b*-PI) or polystyrene-*block*-polybutadiene (PS-*b*-PB) systems blending with PS homopolymers [Fig. 3(a)]. Because of the wet brush characteristics of the blending PS homopolymers, the addition of homopolymers to the lamellae-forming diblock increases the compositional asymmetry to generate curvature at the self-assembled interface [Fig. 3(b)] [74]. Similar scenarios can be applied to the BCPs with asymmetric composition blending with homopolymers to the minor compositions [Fig. 3(c)] [73]. The ordered bicontinuous network phase can also be acquired from the self-assembly of cylinder-forming BCP/homopolymer blends, where the wet brushes are uniformly distributed with the minor microdomains to compensate for the loss of entropic penalty from the forming phases with TPMSs. Theoretical simulations based on the mean-field theory for the distributions of the polymer chains in the self-assembled network phases have also been studied for decades. A common conclusion has been given that the wet-brush-like behaviors of the homopolymer blends can be an effective approach to overcome the packing frustration from the forming network phases, yet excess addition of the additives will result in undesired occurrence of macrophase separation.

Following the concept, a strategy proposed by Court and Hashimoto [75] demonstrated the alternative to compensate for the loss of entropic penalty in binary mixtures of BCP through the *cosurfactant effect*. Those binary mixtures consisting of both diblocks with asymmetric compositions can effectively trigger the spontaneous curvature during

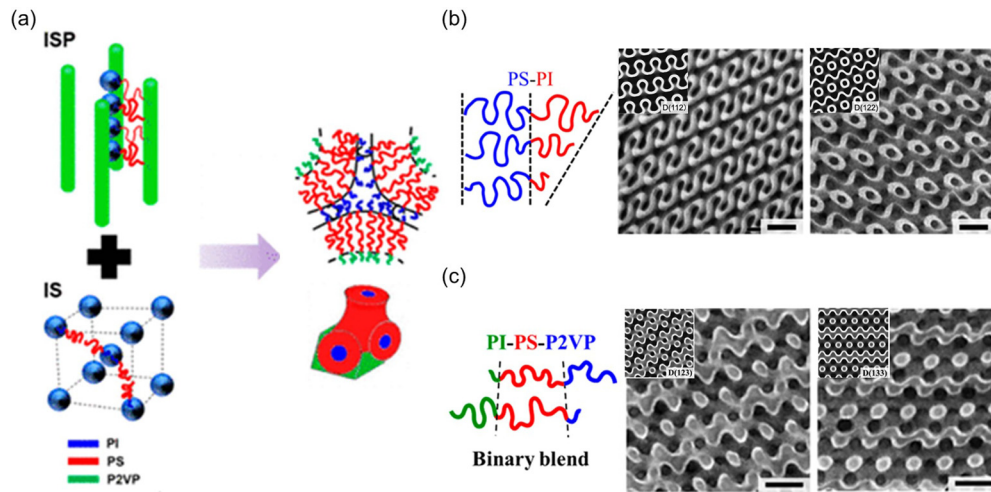


FIG. 4. (a) Illustration of core-shell double gyroid (DG) from binary mixture of highly asymmetric compositions of ABC/AB blends [76]. (b) Transmission electron microscopy (TEM) micrographs of ternary blending from three different chain length of polystyrene-polyisoprene (PS-PI) [55]. (c) TEM micrographs of two triblock copolymer blending [56].

self-assembly, thus potentially giving greater window to the formation of network phases [71]. Asai *et al.* [55] revealed the emergence of the DG phase in binary BCP mixtures and validated the formation of the stable DD phase in ternary blends of three PS-*b*-PI mixtures [Fig. 4(b)]. Moreover, by taking advantage of the rich phase behaviors of the ABC-type triblock terpolymers, the cosurfactant effect can also be applied to the triblocks seeking routes to acquire various network phases. As shown in Fig. 4(a), a core-shell DG can be found in binary mixtures of ABC/AB blends which exhibit highly asymmetric compositions [76]. Apart from the DG phase, a stable alternating DD phase can be found when two triblocks are mixed at particular compositions; note that the intrinsic phase behaviors of the constituted BCPs are far beyond the regions of network phases on the corresponding phase diagrams [Fig. 4(c)] [56]. The intrinsic inconsistency of the chain lengths in the minor phases at particular compositions is expected to fit the deviated curvatures in TPMSs well, which avoids the entropically unfavorable situations of overstretch and compression to polymer chains. As a result, the uniform space filling of polymer chains leads to the rare formation of diamond phases which have been long considered metastable phases [55,56].

B. Multi-BCPs and others

In recent years, the advance in the development of synthetic techniques has allowed wild designs of BCP conformations to explore fascinating and unique phase behaviors. In a typical BCP system, there are two controlling factors (segregation strength and constituted compositions) that govern the phase behaviors, no matter whether those are in equilibrium or metastable phases. However, the introduction of the topology design to block sequences and molecular conformations led to dizzying phase complexity. For BCPs with alternating sequences in linear extension, named *multi-BCPs*, those can be successfully synthesized through step-growth polymerization. Like the alternating complexity of peptides in proteins, the sequence and sizes of each block dominate the final geometry

of packing symmetry of the self-assembled phase [77]. The DG phase can be found in polyethylene (PE)-like materials containing sulfonate groups in alternating sequences upon the melting of semicrystalline PE blocks [Fig. 5(a)] [78]. The short but flexible PE chains due to the semicrystalline characteristic and the monomerlike sulfonate group lead to the formation of continuous sulfonate gyroid networks and PE matrix. Moreover, the intensive intermolecular interactions among the ionic sulfonate group allow the formation of ionic aggregate, assisting in the stabilization of packings within the trigonal nodes [79]. There are more emerging categories of BCPs, especially for the bottlebrush BCPs [80]. The bottlebrush BCPs show highly branched topology consisting of different types of grafted side chains on a linear backbone, featuring rapid self-assembly into highly ordered states in large dimensions [81,82]. The controlling of the length of the backbones or the side chains, sequence of the side chains, and the relative ratios of side chains can generate various nanostructures including the desired network phase [35,83,84]. A mix-and-match of the bottlebrush to the random coil further expands the flexible adaptability of soft matter to the creation of network phases. As shown in Fig. 5(b), Park *et al.* [35] demonstrated the architectural effect from the bottlebrush can profoundly impact the stability of the gyroid based on the consideration of conformational asymmetry. Because of the difference in the stiffness of the coils and the backbone in the bottlebrush, the coils in the minor phase will be confined at the center of the trigonal node (DG) which alleviates the packing frustration. The mix-and-match combinations of the designs of molecular architectures suggest the favorable formation of curvatures, providing more accessibility to the network phases through precise synthetic routes of BCPs in combination with the study of topology.

In contrast with the forming ordered network phases through self-assembly of BCPs, there are other alternatives to fabricate the disordered network nanostructures by the *in situ* operations of polymerization and phase separation simultaneously [85,86]. By taking advantage of the intrinsic incompatibility of the constituted components, the

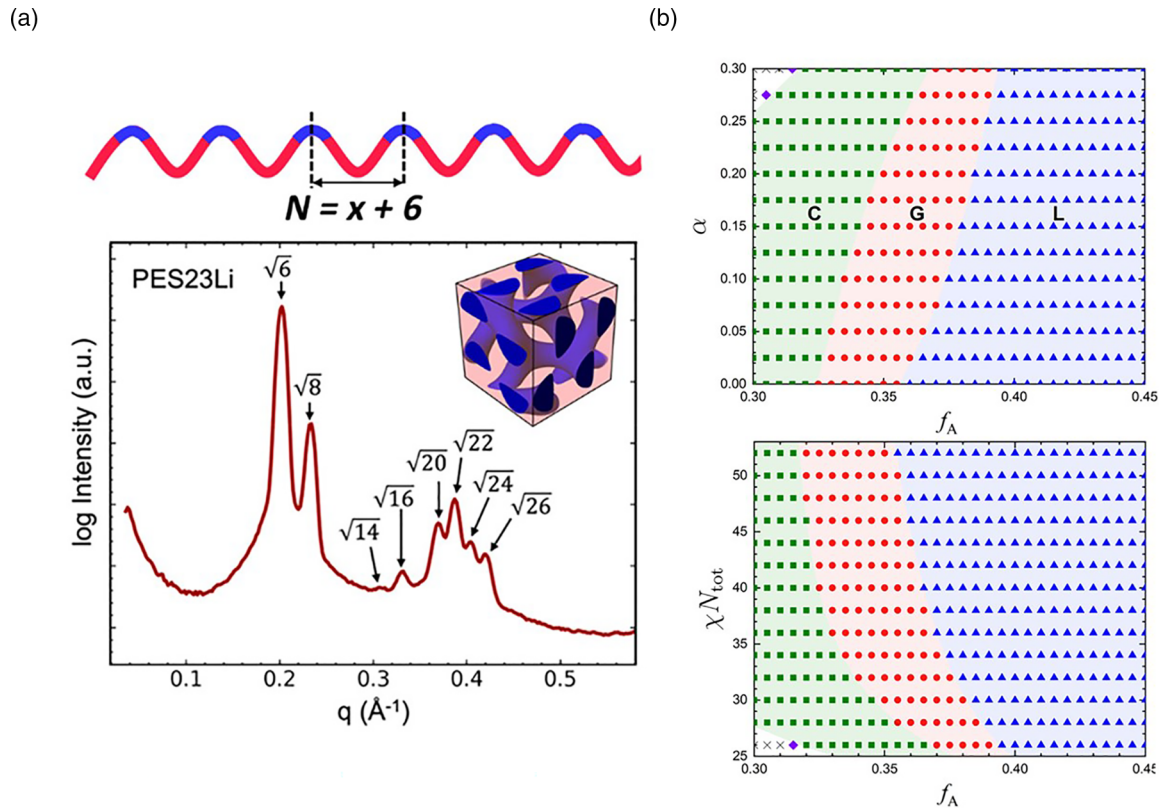


FIG. 5. (a) One-dimensional small-angle x-ray scattering (SAXS) profile of polyethylene (PE) alternating with sulfonate groups by thermal annealing [78]. (b) Phase diagram at fixed $\chi N_{\text{tot}} = 26$ (top) and $\alpha = 0.3$. The stability regions of lamellae, gyroid, and cylinder phases are labeled [35].

spontaneous occurrence of spinodal decomposition of the two-phase mixtures will result in the formation of bicontinuous polymeric frameworks, at which the average spacing of networks is dominated by the sizes of the macromolecular chain transfer agent (macro-CTA) introduced into the system, as show in Figs. 6(a) and 6(b) [85]. Undergoing crosslinking during polymerization, the formed bicontinuous framework by spinodal decomposition can be frozen and preserved after the termination of the synthesis [Fig. 6(c)] [87]. In comparison with the ordered phases with uniform feature sizes from the self-assembly of BCPs, the dynamic procedures of polymerization-induced phase separation indeed expand the category to the creation of disordered network nanostructures via a one-step synthesis of randomly copolymerization of BCPs.

IV. KINETIC CONTROL FOR SELF-ASSEMBLY OF BCPS

Following the ideal physics principles, the polymer coils are physically redistributed from the competition between enthalpic and entropic origins to reach the global minimum during the self-assembly of BCPs to give the formation of diverse phases. By taking advantage of the viscoelastic characteristic of polymers, the multistep transitions (crystal/glass, rubber, and melt) gives wide accessibility to control the progress of self-assembly which results in the feasibility to capture phases at the local minimum along the free-energy diagram [88–90]. In this paper, based on the previous studies, a simple route to acquire the network phases in the metastable

state is thus proposed with the understanding of the possible forming mechanisms. For instance, the introduction of additional components, such as solvents or homopolymers, overall alters the developing process of microphase separation; in addition, the dynamic changing on the surroundings can also create fluctuations on the alignment of polymer chains, resulting in temporarily energy-favorable phase behaviors. The factor of kinetics will be included in the discussion to clarify the origins of diverse metastable network phases which can be captured along the evolution of phase transitions from homogeneous mixing before reaching the thermodynamically favorable equilibrium. The understanding of fundamental facets for the phase behaviors of BCP self-assembly from the nonconventional viewpoint and state-of-the-art methodologies of processing BCPs through common techniques for the accessibility of self-assembled network phases will be promising to facilitate academic activities on developing methods to acquire metastable network phases for futuristic applications such as multifunctional metamaterials because of deliberate network structuring.

A. Effect of solvent selectivity on phase behaviors of BCPs

Traditionally, the so-called classical ordered phases of BCPs were prepared by achieving the order-disorder transition from microphase separation [1–3,91]. Heat is often used for governing the progress of self-assembly due to the temperature-dependent segregation strength (χN), especially for χ [1,3,92]. However, it could be difficult for

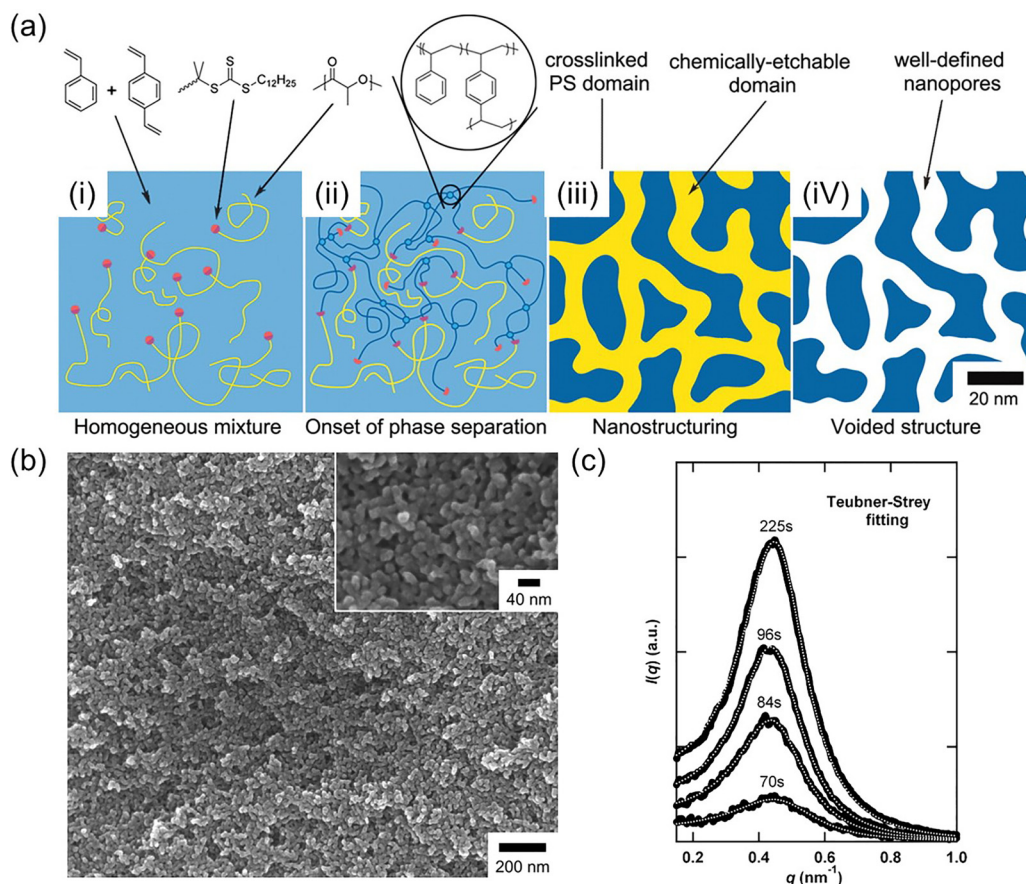


FIG. 6. (a) Illustration of nanoporous monolith after polymerization-induced microphase separation process [85]. (b) Scanning electron microscopy (SEM) micrograph of the nanoporous monolith [85]. (c) One-dimensional small-angle x-ray scattering (SAXS) profiles of 70, 84, 96, and 225 s copolymerization at 338 K [87].

systems containing degradable compositions and/or high molecular weights [19,93]. The processing can be prepared by adding a solvent instead, alleviating the unfavorable monomer-monomer interactions. The addition of diluents, low-molecular-weight components, provides a higher degree of freedom to the condensed matter, resulting in more complicated phase behaviors. Lodge *et al.* [94], Huang and Lodge [95], and Hanley *et al.* [96] discussed the phase behaviors of BCPs dissolved in neutral solvents or slightly selective solvents as concentrated solutions, revealing the formation of BCPs/solvent micelles which aggregate in anisotropic alignment and grow as an ordered phase step by step during the phase separation [Fig. 7(a)] [96]. SCFT also predicts the evolution of simple ordered phases from lamellae, cylinders, and spheres to micelles or disordered states in the presence of solvents [Fig. 7(b)] [95]. All can be attributed to the reduction of segregation strength being inversely proportional to the contents of solvents [95]. In addition to the portion of solvents in polymer solutions, the selectivity of solvents has been testified as a crucial factor to tune the final phase morphologies. In a commonly studied polystyrene-*block*-polyisoprene (PS-*b*-PI) system, multiple phases could be obtained in the same way as the ones on the well-established phase diagram by changing the selectivity of solvents and the surrounding temperatures from a single asymmetric sample [94]. Though the ordered

phases are observed in a fluidic solution state instead of in condensed matter, the idea of a diluted polymer solution still inspired the use of a solvent to adjust the final phase behaviors.

However, the intrinsic properties of PS-*b*-PI with weak segregation strength due to the low χ value may limit the selections of the solvent. According to the Flory-Huggins theory, $\chi \sim (\delta_A - \delta_B)^2$ [2], where χ is proportional to the difference between the solubilities of the two constituted blocks; that is, the difference between the selectivities of the two polymers could be weak which is far away from the strongly segregated amphiphilic surfactant/water [97–100]. It is thus challenging to give a variety of phases.

To improve the effect of solvent selectivity to the BCPs, a high- χ BCP could be an alternative solution to enrich the phase behaviors of BCPs/solvent mixtures. Lo *et al.* [101] demonstrated a wide variety of phases, including inverted phases, in a silicon-containing BCP, polystyrene-*block*-polydimethylsiloxane (PS-*b*-PDMS), with the use of multiple kinds of solvents for solution casting. The effects of the selectivity of a solvent in a high- χ PS-*b*-PDMS—strongly PDMS-selective (methylcyclohexane), weakly PS-selective (toluene), and strongly PS-selective solvent (1,2,3,4-tetrahydronaphthalene)—were systematically examined; Fig. 8 shows the corresponding

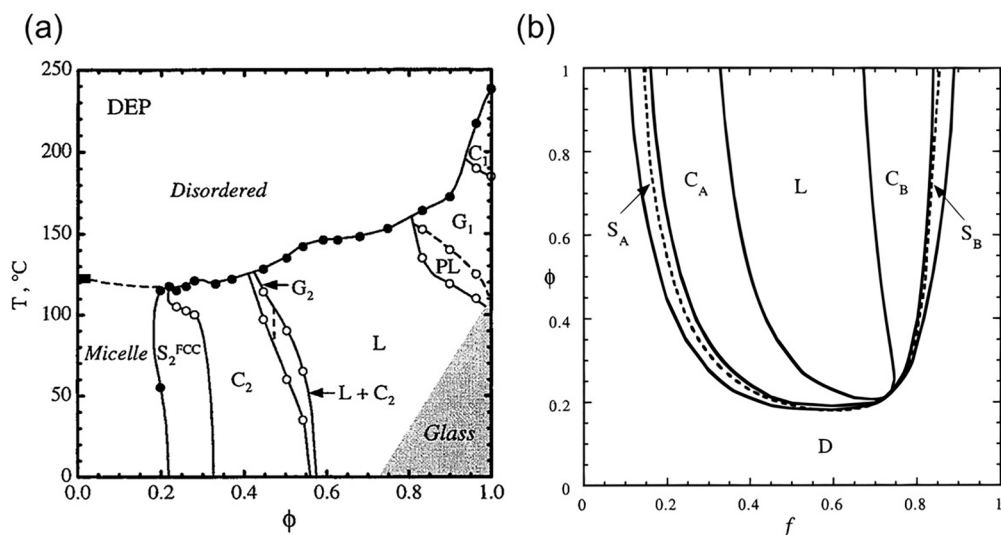


FIG. 7. (a) Phase diagram of polystyrene-*block*-polyisoprene (PS-*b*-PI) as a function of temperature T and concentration of polymer in solution (volume fraction ϕ) of diethyl phthalate (DEP) [96]. (b) Two-dimensional phase map for a block copolymer solution with $N = 200$, $\chi_{AS} = 0.6$, $\chi_{BS} = 0.4$, and $\chi_{AB}N = 45.0$ [95].

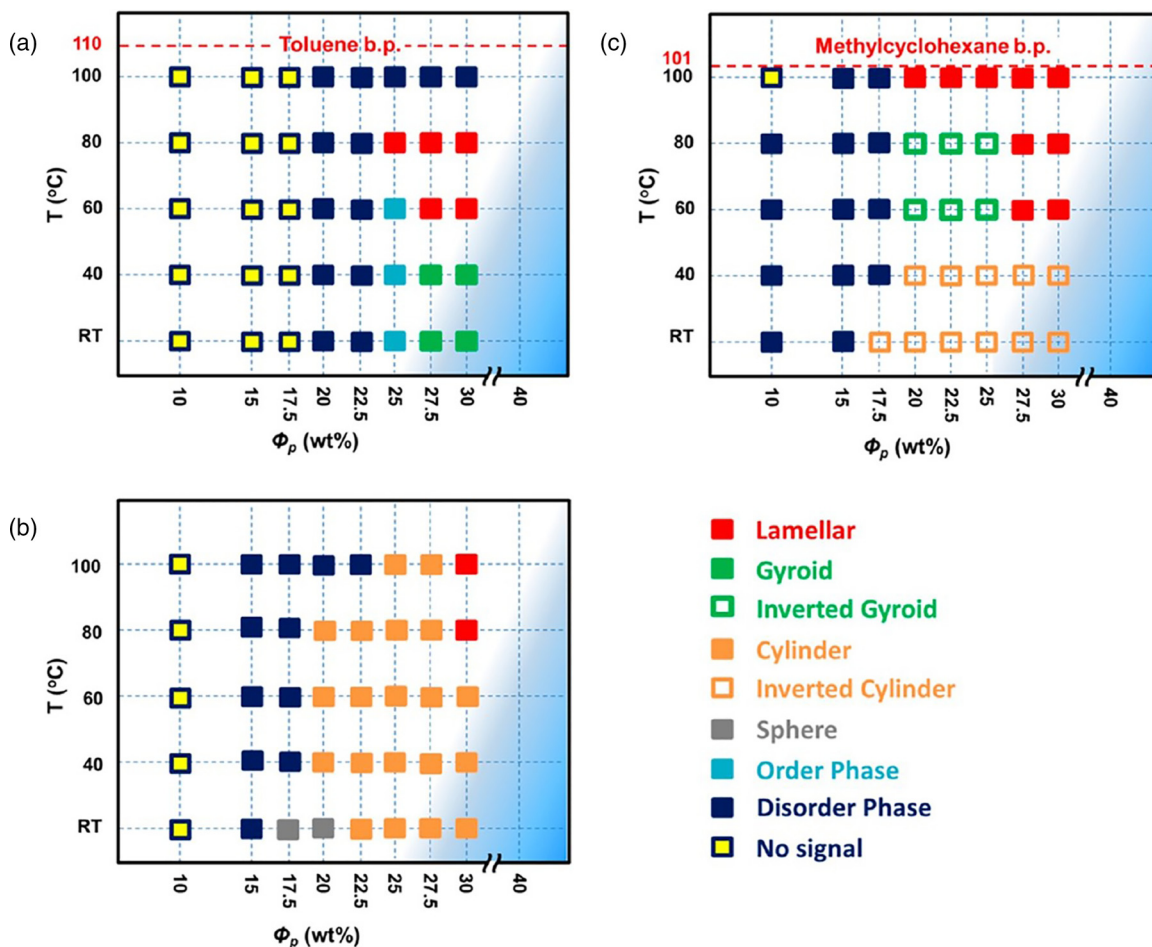


FIG. 8. Phase diagrams for polystyrene-*block*-polydimethylsiloxane (PS-*b*-PDMS) in different selective solvents as a function of temperature (T) and polymer concentration (ϕ) in (a) toluene solution, (b) 1,2,3,4-tetrahydronaphthalene, and (c) methylcyclohexane. The corresponding phases for each symbol are listed at the lower right corner [101].

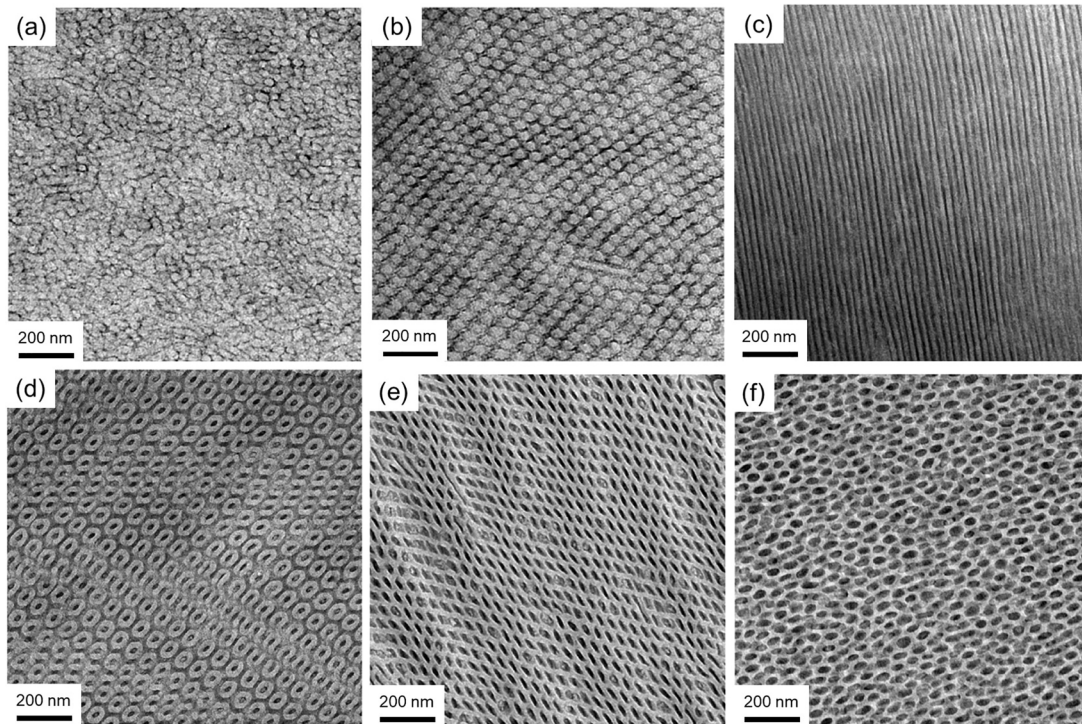


FIG. 9. Transmission electron microscopy (TEM) micrographs of the self-assembled polystyrene-*block*-polydimethylsiloxane (PS-*b*-PDMS) acquired by using (a) hexane, (b) methylcyclohexane, (c) cyclohexane, (d) toluene, (e) chlorobenzene, or (f) 1,2-dichloroethane as a solvent for solution casting [101].

phase behaviors. In line with the results from Huang *et al.* [95] and Hanley *et al.* [96], the dilute polymer solution in a weakly selective solvent has a disordered state, where a homogeneous mixture can be found in the whole measured range of temperatures. As the concentration increases, micelles are first formed and become aggregates, while no obvious signals of microphase separation can be traced by small-angle x-ray scattering (SAXS). The ordered phases could be found in a concentrated solution as the χ value rises near the vitrified point of BCPs when the monomer-monomer interaction impedes the mobile freedom due to the viscoelastic characteristic of polymers. Multiple reflections appear at the relative q values of $\sqrt{6}:\sqrt{8}:\sqrt{14}:\sqrt{16}:\sqrt{22}$ that perfectly match the scattering profile of a DG phase. A DG phase is, therefore, found at low temperature, while the intrinsic phase, lamellae, will only be acquired at high temperature. A solvent with stronger selectivity than PS (1,2,3,4-tetrahydronaphthalene) gives similar results, whereas the effective volume fraction of PDMS (f_{PDMS}^v) is significantly reduced; hexagonally packed cylinders and even spheres can be obtained. Furthermore, in comparison with the one using toluene, the larger discrepancy between the solubilities among the solvent and BCPs may slightly increase the χ value in the polymer solution and facilitate microphase separation at lower concentration. On the contrary, the PDMS-selective solvent (methylcyclohexane) will revolve the phase behaviors due to the studied system with nearly symmetric composition [Fig. 8(c)]. Inverted phases can be observed when PDMS selective solvents are used for controlled self-assembly. Not only the inverted cylinders [Fig. 9(b)] but also the inverted gyroid appears at

specific conditions, suggesting the overswelling of PDMS flips over the curvatures by overturning the volumetric asymmetry of the building blocks in solvents, meanwhile, retaining sufficient segregation strength for self-assembly owing to the intrinsically high χ value. It is noteworthy that the acquired phases mostly can be preserved as the solvent evaporates, suggesting that the reached equilibrium state of BCP/solvent mixtures in the solution state can be fixed when the polymer coils are incapable of rearranging. Through mixing and matching of solubility to the constituted components, PS and PDMS, multiple selections of solvents are therefore used for controlled self-assembly of PS-*b*-PDMS, as summarized in Fig. 9. The adjustable effective volume fractions of the BCPs provide wide accessibility to control the phase behaviors in solutions by different selections of solvents followed by solvent evaporation to acquire the metastable phases as the self-assembled BCPs become vitrified.

B. Kinetic routes to formation of metastable network phases

As discussed above, it is feasible to preserve various phases from the self-assembled BCP/solvent mixtures in the solution state followed by removal of the solvent. The different stages of the concentration create diversity of the effective χ values and, most crucially, the volumetric ratios; therefore, order-order transition may occur during the evaporation of the solvent (Fig. 8). Generally, in the field of material science, cooling is a common approach to quench specific phases during the progress of order-order transition [102]. For BCP/solvent mixtures, the low melting point of the

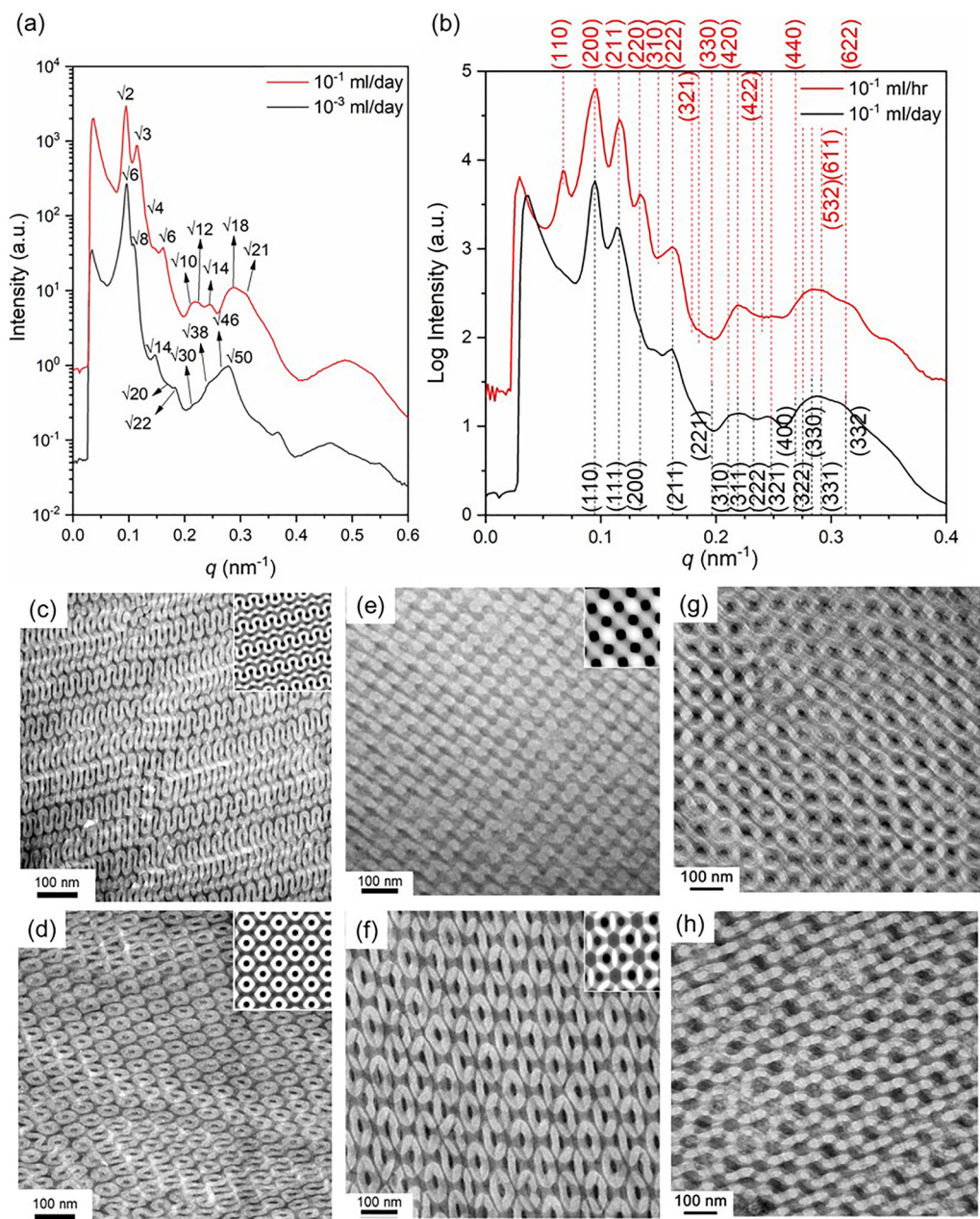


FIG. 10. One-dimensional small-angle x-ray scattering (SAXS) profiles of polystyrene-*block*-polydimethylsiloxane (PS-*b*-PDMS) by controlled self-assembly using chloroform under (a) slow and moderate and (b) moderate and fast evaporation rates. Transmission electron microscopy (TEM) micrographs of the acquired self-assembled PS-*b*-PDMS from (c) and (d) slow, (e) and (f) moderate, or (g) and (h) fast evaporation rates [105].

mixture, however, can be a harsh requirement for quenching due to the use of organic liquids for controlled self-assembly at regular surroundings. By taking advantage of the unique viscoelastic characteristic of polymer solutions, polymers will be vitrified at particular conditions (i.e., glassy state); the mobility of polymer coils will be prominently suppressed [103,104]. Fast evaporation of the solvent is possible to kinetically capture the intermediate before it transforms into the equilibrium state during the proceeding development of order-order transition as the solvent evaporates. An alternative measure proposed by Chang *et al.* [105] may provide insights into the processing of BCP self-assembly. A high- χ BCP,

PS-*b*-PDMS with nearly symmetric composition, is taken as a representative system for examination of corresponding kinetic factors on phase behaviors during the controlled self-assembly. A weakly PS-selective solvent, chloroform, is selected, following the strategies as reported previously. A DG phase is formed, as evidenced by the scattering profile [Fig. 10(a)] which fits an ideal pattern at relative q values of $\sqrt{6}:\sqrt{8}:\sqrt{14}:\sqrt{20}:\sqrt{22}$. Representative projections of a DG phase along [110] and [211] under transmission electron microscopy (TEM) [Figs. 10(c) and 10(d)] further validate the formation of the DG phase while using chloroform as a solvent for controlled self-assembly at a slow evaporation

rate (10^{-3} mL/d). Abundant time is provided for the polymer solution to reach equilibrium at a given effective volume fraction of PS-*b*-PDMS before the evaporation of the solvent. Surprisingly, things go beyond expectation as the evaporation rate of chloroform accelerates. Different patterns of projections are observed under TEM, implying the occurrence of order-order transition to a new phase; the fingerprints of the corresponding scattering profile also change [Fig. 10(a)]. Chessboardlike and wagging patterns are identified, resembling the projections of a DD phase along [100] and [311] [Figs. 10(e) and 10(f)]. Moreover, the labeled reflections at the relative q values of $\sqrt{2}:\sqrt{3}:\sqrt{4}:\sqrt{6}:\sqrt{10}$ prove the order-order transition to a DD phase at a moderate evaporation rate (10^{-1} mL/d). The 3D visualization by electron tomography clearly exhibits the fourth struts on the trigonal planar structures, thus becoming tetrahedral nodes (tetrapod) in the same way as a diamond structure [28,45]. It is noteworthy that the DD phase is viewed as a metastable network phase instead of an equilibrium state marked on the phase diagrams. The fluctuating environments of polymer solutions disturbed by the moderate evaporation rate of a selective solvent may provide access to the formation of metastable network phases instead of equilibrium phases. Network phases with lower metastability are expected to be kinetically captured under extreme conditions. As the evaporation rate drastically rises to 10^{-1} mL/h, unique real-space images are acquired where nodes with bulky sizes can be identified [Figs. 10(g) and 10(h)]. Moreover, in comparison with the acquired DD phase, additional reflections in the reciprocal-space image sharply appear at the low- q region, and each reflection corresponds to Miller planes when $h + k + l = 2N$ [red lines in Fig. 10(b)]. The reconstruction reveals the formation of a double-network phase composed of repeating units with six struts (hexapod), evidencing the existence of a Schwarz primitive minimal surface, and those unexpected projections were attributed to the projections viewed along [100] and [111] [Figs. 10(g) and 10(h)]. The formation of a DP phase is confirmed, accounting for the reflections from $(110)_{DP}$ and $(220)_{DP}$ at the low- q region. Moreover, there are overlapping peaks from the DP to the DD such as $\sqrt{4}:\sqrt{6}:\sqrt{12}$ from the reflection planes of $(200)_{DP}$, $(211)_{DP}$, and $(222)_{DP}$, implying the coexistent formation of DP and DD phases at the same time. A 3D reconstruction image covering a larger area is acquired in which the hexapod building units from the DP and the tetrapod from the DD phase can be visualized, proving the coexistence of DP and DD phases through controlled self-assembly of PS-*b*-PDMS under a fast evaporation rate (10^{-1} mL/h); the grains of the DP phase are surrounded by the DD matrix. As a result, the order-order transition between the two metastable network phases can be observed. It is noteworthy that the formation of such metastable network phases is rarely observed in BCPs. To achieve the isolation of the DP phase from the coexistence of two phases, a faster evaporation rate is attempted to kinetically preserve the forming DP phase before the undergoing transition to the DD phase during self-assembly. The populations of the DP phase do increase, yet the DD phase can still be observed; further accelerating the evaporation of the selective solvent results in a disordered network. The fluctuated states similar to spinodal decomposition at low

concentration are captured, as shown in Fig. 8, consistent with the mechanism for the formation of a network phase from an initial state showing homogeneous mixing of BCPs [3]. Even though PS-*b*-PDMS shows a high χ value, the overswelling in the polymer solution reduces the final segregation strength drastically; as a result, the BCPs cannot be self-assembled into ordered phases [95,106]. Furthermore, the ultrafast removal of the solvent leaves little time for rearrangement of the polymers before the polymer solution dries out; no ordered phase can be formed. Conclusively, three network phases, including the DG and two metastable network (DD and DP) phases can be acquired by controlling the evaporation rate of the PS-selective solvent during the controlled self-assembly.

To further investigate the thermodynamic stabilities of the forming network phases, a temperature-resolved *in situ* SAXS experiment was carried out. According to the prediction by simulations, network phases with higher strut numbers will encounter a higher degree of packing frustration, demonstrating lower metastability [37,47]; the one with coexistent DP and DD phases is thus selected as the initial state in the experiment [Fig. 11(a)]. The characteristic reflection in the low- q region for the suggested coexistent DP and DD phases can be clearly identified at low temperature. An order-order transition occurs as the temperature rises >130 °C, at which a drop in intensity for $(110)_{DP}$ can be recognized. Owing to the high packing frustration in the DP phase, that implicitly indicates the occurrence of a transition from the DP to the DD phase, consistent with the different phase behaviors obtained through controlled self-assembly under different evaporation rates. As a result, a low energy barrier for the DP-DD transition is expected. As the temperature reaches 150 °C, the reflections from $(110)_{DP}$ and $(110)_{DD}$ start to broaden and approach each other simultaneously, suggesting the occurrence of order-order transitions from the coexistent DP and DD phases to a new phase. The major change of the reflections of the DP and DD phases occurred at 160 °C when the mixed phases were extinct. A significant reflection emerges at the low- q region, suggesting the completion of the phase transformation as the temperature reaches >160 °C. Detailed analysis of the significant reflection in the scattering profile reveals the formation of the DG phase. The degree of packing frustration of the ordered network phases indeed reduces as the thermal annealing proceeds. The characteristic reflection planes for the DG were marked as the red dashed lines at the relative q values of $\sqrt{6}:\sqrt{8}:\sqrt{14}:\sqrt{18}:\sqrt{22}:\sqrt{32}$. Real-space imaging by TEM further evidenced the formation of DG, as shown in Fig. 11(b). Moreover, based on the reconstruction results, the transition zones from the DP to the DD phase and those from the DD to the DG phase could clearly be observed; no evidence for the phase transition from the DP to the DG phase can be identified. Eventually, the phase transition stops, as it transforms into a lamellae phase according to its intrinsic composition. In comparison with the predicted D-G-P phase transitions based on enthalpy-driven Bonnet transformation, the packing frustration from the highly stretched polymer chains to the center of the nodes results in an entropic penalty for the phase transitions. Considering the size of the nodes for the three network phases, the bulkiest dimension of the DP phase thus shows the lowest metastability; the DD phase with a smaller size of

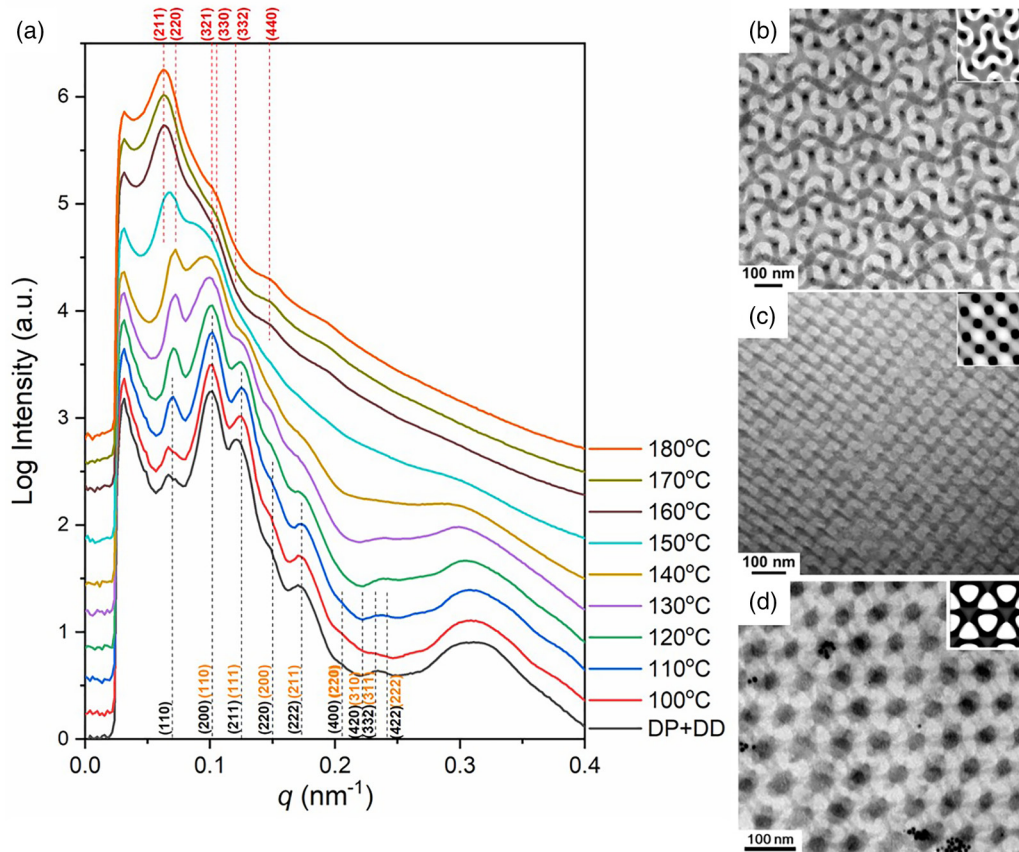


FIG. 11. (a) Temperature-resolved *in situ* one-dimensional (1D) small-angle x-ray scattering (SAXS) profiles of the self-assembled polystyrene-*block*-polydimethylsiloxane (PS-*b*-PDMS) under fast evaporation rate. The red dashed lines are the reflection planes referred to $Ia\bar{3}d$ [double gyroid (DG)]. The orange brackets are the reflection planes referred to $Pn\bar{3}m$ [double diamond (DD)] at which an additional peak could be clearly identified in the low- q region. The black dashed lines are the reflection planes based on double primitive (DP) phase with $Im\bar{3}m$. Transmission electron microscopy (TEM) micrographs of the self-assembled PS-*b*-PDMS during different stages of thermal annealing: (b) The DG phase quenched at 180 °C and the initial state of the coexistent (c) DD and (d) DP phases [105].

nodes shows slightly higher metastability. The trigonal planar junction with nearly uniform curvature and thickness has the least degree of packing frustration, in line with the speculation that the smallest deviation on curvature from CMC suggests the better metastability. Accordingly, we speculate that a polymer with freely stretching chains (especially PDMS) might be kinetically trapped via the fast evaporation of a selective solvent (chloroform), where the PDMS blocks might extend into the interior core of the junctions even with the loss of entropy from such a high-strut-number network texture (i.e., DD and DP phases). As temperature rises, thermal energy attenuates the χ value, inducing fluctuations on the interfaces that relieve the concentrating stress, resulting in transformation into the DG phase.

C. Metastable network phases in thin-film state

Solvent annealing is a feasible way to obtain well-ordered structure in a film state and takes less time to achieve the aimed morphology than thermal annealing [107–110]. Also, solvent annealing has been widely studied in controlling annealing processes followed by different evaporation rates. Here, the feasibility to carry out controlled self-assembly of PS-*b*-PDMS for metastable network phase fabrication can

also be achieved by solvent annealing. Owing to the narrow window for network phases, a PS-selective solvent was used to capture the metastable network phase from a thermodynamically stable lamellae phase. By taking advantage of easy tuning of the flow rate of the PS-selective solvent, gyroid- and diamond-structure monoliths can be formed in the thin-film state.

With the use of a PS-selective solvent, swellings of two constituted blocks are distinguished from each other. To stimulate the condition for the solution casting process, 10 and 20 mL/min were used to represent low and high evaporation rates. As shown in Fig. 12(a), the swelling ratio of a PS homopolymer film remains the same under two different flow rates, while the solvent annealing uses chloroform as a good solvent for PS. On the contrary, a discrepancy between swelling ratios of the PDMS homopolymer film was found, as shown in Fig. 12(b). Based on the equation, discrepancy between swelling ratios of PS and PDMS would cause the different effective volume fractions of PDMS, leading to the formation of network structures:

$$f_{\text{PDMS}}^{\text{eff}} = \frac{f_{\text{PDMS}}^{\text{in}} \times SR_{\text{PDMS}}}{f_{\text{PDMS}}^{\text{in}} \times SR_{\text{PDMS}} + f_{\text{PS}}^{\text{in}} \times SR_{\text{PS}}} \quad (1)$$

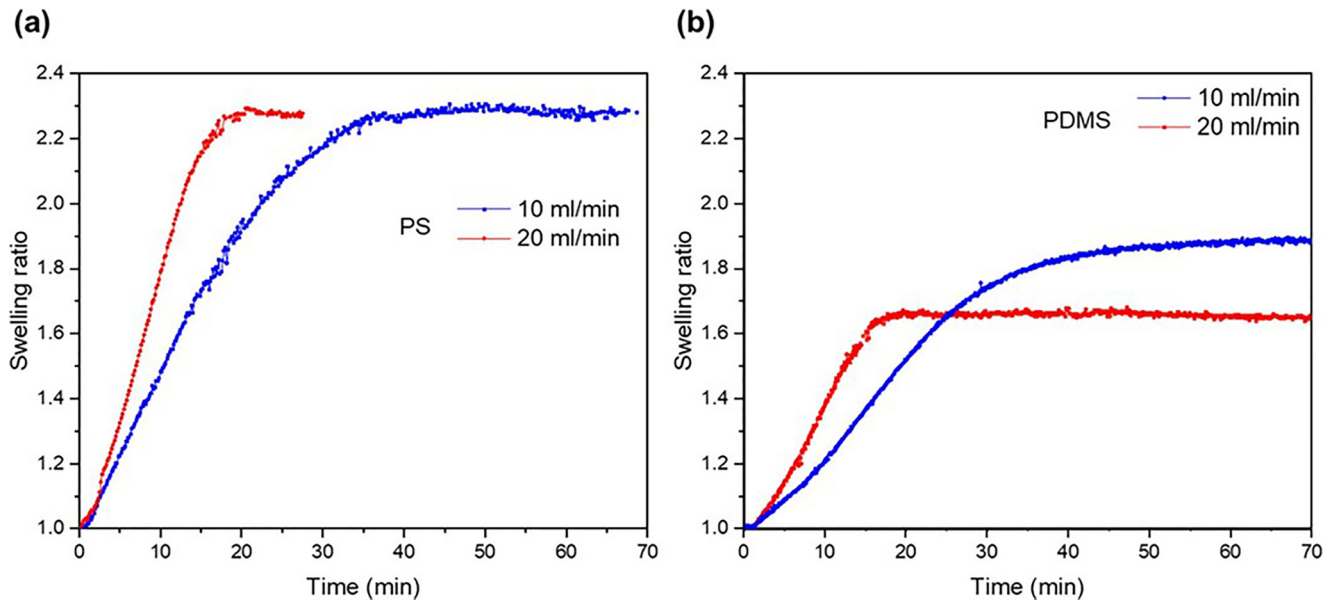


FIG. 12. Swelling ratios of (a) polystyrene (PS) and (b) polydimethylsiloxane (PDMS) homopolymer film at 10 and 20 mL/min. Equilibrium swollen thickness was determined by averaging the last 50 data points (thickness variation within ± 2 nm). Each thickness profile of homopolymer films during solvent annealing at the same flow rate was measured three times [111].

where f_{PS}^{in} and f_{PDMS}^{in} are the intrinsic volume fractions of PS (0.58) and PDMS (0.42) in PS-*b*-PDMS. Here, SR_{PS} and SR_{PDMS} are the swelling ratios of PS and PDMS homopolymer films at the identical flow rate, respectively.

PS-*b*-PDMS with the same composition as reported previously will be used [105]. PS-*b*-PDMS film was prepared by dip-coating with the PS-selective solvent chloroform. As shown in Fig. 13(a), amorphous network formation was achieved after dip-coating, giving the preliminary structure of the thin film. The effective volume fraction of PDMS would gradually decrease during the solvent annealing pro-

cess. As a result, the network structure could be acquired from a single-component lamellar phase. Controlling the flow rate at 10 mL/min, different morphologies could be traced at different solvent annealing times. As time goes by, film morphology transfers from the amorphous network phase to the long-range ordered network phase. As shown in Fig. 13(c), a well-ordered network structure can be captured after a longer annealing time. A typical DG phase $(211)_{DG}$ is formed and can be confirmed by the corresponding stimulation. Furthermore, the relative q values at $\sqrt{6} : \sqrt{8} : \sqrt{14} : \sqrt{22} : \sqrt{50}$ from the SAXS experiment [Fig. 13(e)(iii)] also show the

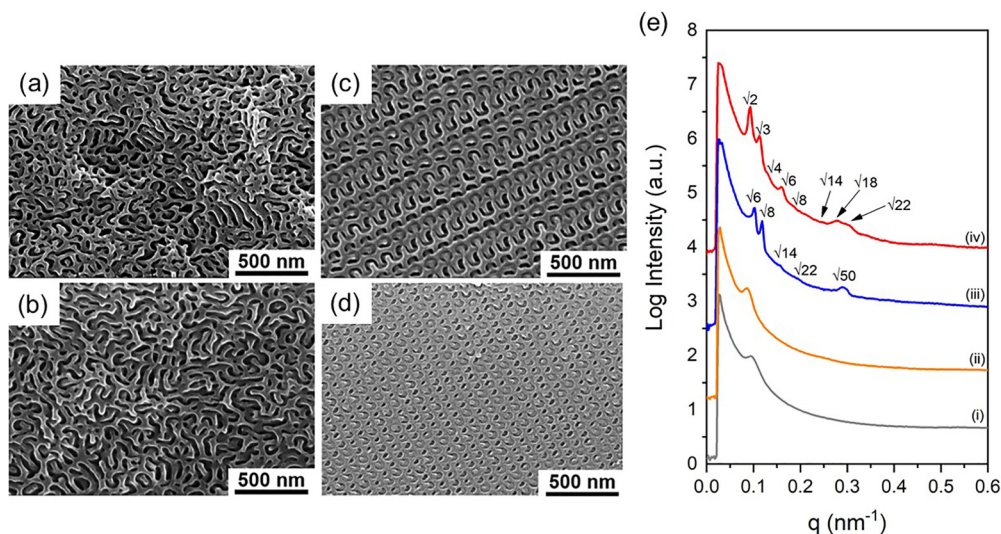


FIG. 13. Field-emission scanning electron microscopy (FESEM) micrographs of (a) dip-coated polystyrene-*block*-polydimethylsiloxane (PS-*b*-PDMS) films and after solvent annealing with chloroform for (b) 30 h and (c) and (d) 60 h at flow rates of 10 and 20 mL/min, respectively. (e) Small-angle x-ray scattering (SAXS) profiles of (i) dip-coated PS-*b*-PDMS films and (ii) after solvent annealing for 30 h and (iii) and (iv) 60 h at flow rates of 10 and 20 mL/min, respectively [111].

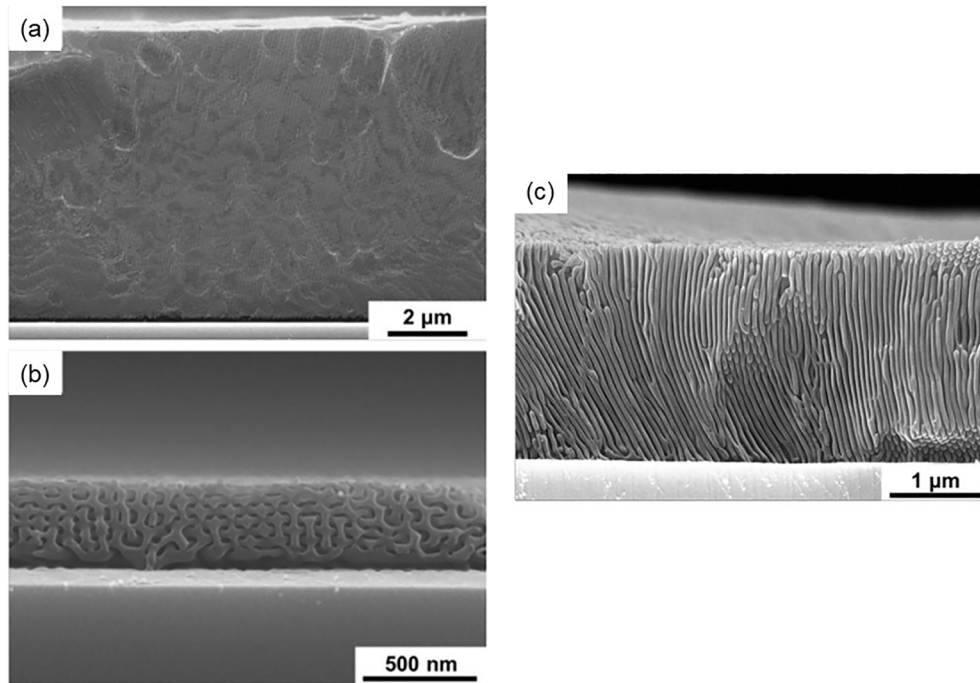


FIG. 14. Field-emission scanning electron microscopy (FESEM) micrographs of double diamond structure with thicknesses of (a) 10 μm and (b) 500 nm. (c) FESEM micrographs of cylinder structure after solvent annealing for 20 h at the flow rate of 30 mL/min [111].

DG phase, which is consistent with the SEM micrographs. By slightly tuning the flow rate to 20 mL/min, morphological development forms a disorder phase to the other network phase. Compared with the DG phase, this network phase is significantly different, as shown in Fig. 13(d). The relative q values at $\sqrt{2} : \sqrt{3} : \sqrt{4} : \sqrt{6} : \sqrt{8} : \sqrt{14} : \sqrt{18} : \sqrt{22}$ from the SAXS experiment [Fig. 13(e)(iv)] are not consistent with DG. Referring to stimulation images, the DD structure is evidenced, and Fig. 13(d) shows the imaging from a DD structure with a $(211)_{\text{DD}}$ projection.

To investigate thickness effects, the so-called confinement effect, on the morphology, PS-*b*-PDMS films with various thicknesses were prepared. DD structures can be achieved in a wide range of thicknesses, with the highest reaching 10 μm and the lowest going down to 500 nm, as shown in Figs. 14(a) and 14(b). When the thickness narrows down <500 nm, only disordered network structures can be found, and dewetting problems would be a major challenge during solvent annealing.

Based on the previous measurement of the swelling ratios of homopolymers under different flow rates of chloroform for solvent annealing, the effective volume fraction of PDMS (f_{PDMS}^v) can be estimated. It is calculated that the f_{PDMS}^v is ~ 0.37 for the flow rate at 10 mL/min and ~ 0.35 at 20 mL/min based on Eq. (1). The difference between swelling ratios of the PDMS homopolymer film at 10 and 20 mL/min causes the different f_{PDMS}^v 's, leading to formation of DD and DG phases. It is hard to change f_{PDMS}^v from samples with an intrinsic network phase to achieve various network structures due to slight difference in volume fractions between network phases. According to the tendency of swelling ratios for PS and PDMS, it is expected that the swelling ratio of PDMS will further decrease after the flow rate increases to 30

mL/min; as a result, f_{PDMS}^v will be even lower at the swollen state than before. Controlling the flow rate at 30 mL/min for 20 h, a rodlike structure can be observed from the SEM cross-section view, indicating the formation of a cylinder, as shown in Fig. 14(c). Conclusively, a simple method is proposed to overcome the challenge of the narrow window of network phases and achieve network structures. It is possible to acquire DD and DG structures in the thin-film state from lamellae-forming PS-*b*-PDMS by tuning the flow rate to lead different swellings of PDMS during solvent annealing followed by fast evaporation (rapid rate for removal of solvent). Those results further generalize the phase behaviors of high- χ PS-*b*-PDMS to acquire metastable network phases by controlled self-assembly.

V. TOPOLOGICAL EFFECT ON PHASE BEHAVIORS OF STAR-BCPS

The controlled self-assembly of PS-*b*-PDMS was greatly affected by the selection of solvents and the corresponding kinetic evaporation of the solvent, giving unique phase behaviors that provide the feasibility to acquire metastable phases, especially for the metastable network phases [101,105]. The flexible coil-coil polymer chains of both constituted blocks in a concentrated polymer solution give high plasticity for extension and compression to be sculptured into periodic curvatures. Subsequently, the mesoscale network phases can be vitrified through kinetic control of evaporation of the selective solvent, while the large interaction parameter gives rise to the possibility for creating a sharp interface from microphase separation, giving well-defined ordered phases. The processing indeed expands the windows for network phases, whereas the forming network structures are all viewed as

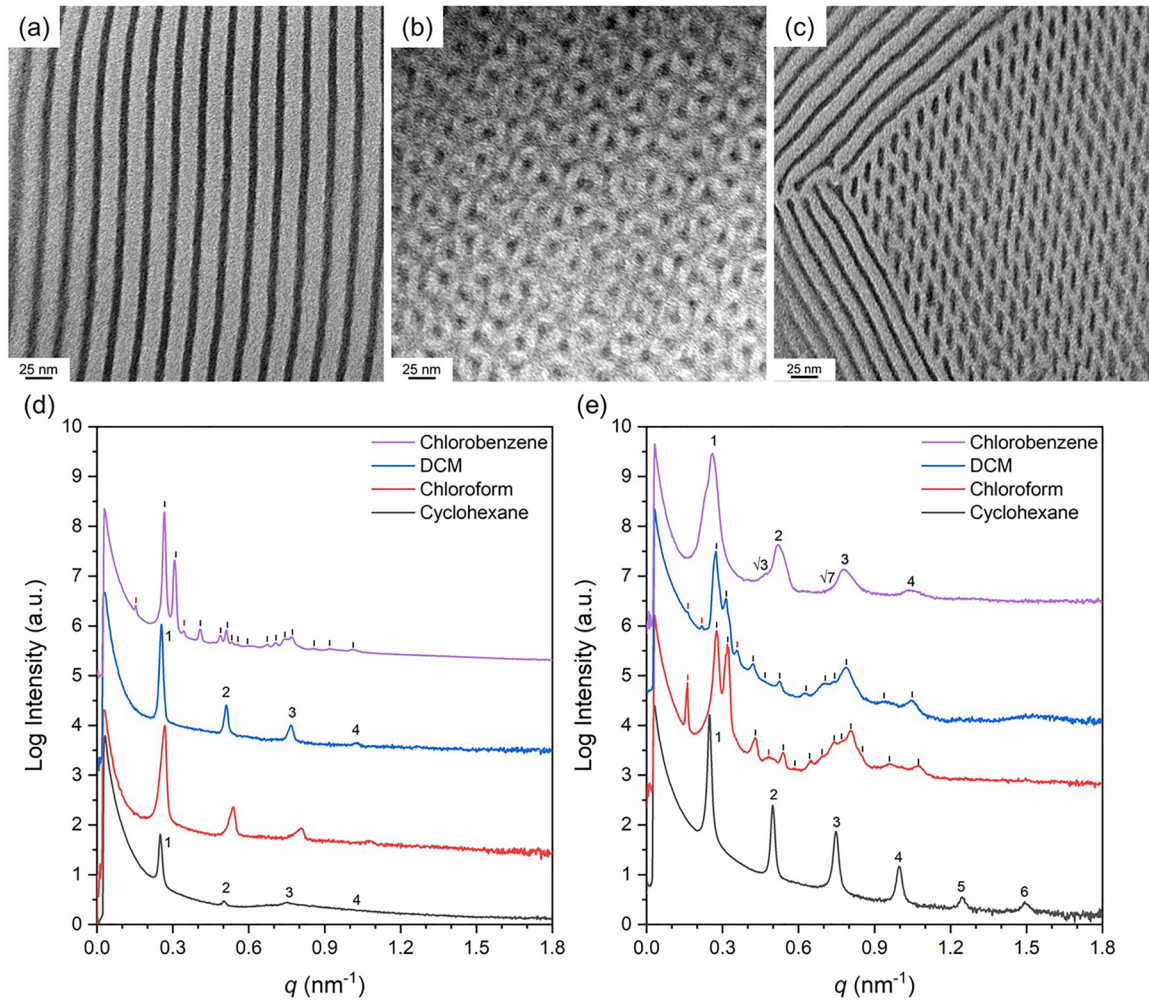


FIG. 15. Transmission electron microscopy (TEM) micrographs of the self-assembled star-block by using (a) cyclohexane, (b) dichloromethane (DCM), and (c) chlorobenzene for controlled self-assembly. One-dimensional small-angle x-ray scattering (SAXS) profiles of the self-assembled (d) diblock and (e) star-block prepared by solvent (cyclohexane, chloroform, DCM, and chlorobenzene) with different selectivity under slow evaporation rate (~ 0.1 mL/d).

metastable states which could be easily transformed into other local minima along the Gibbs free energy diagram because of the high packing frustration of the metastable networks. In the previous section, the primary stage, the DP phase with a large node dimension (i.e., high entropic penalty) cannot be isolated from the DD matrix. The strong segregation strength of PS-*b*-PDMS slightly promotes the extension of polymer chains from the interface when the two constituted blocks bear a high χ value. Although the elastic PDMS chains stretch greatly to reach the interior core for overcoming the packing frustration, the high entropic penalty indeed impedes the formation of the nodes (hexapod) with the larger diameter as compared with the trigonal planar structures [47]. To solve this problem, ideas combining designs of the architecture of BCPs were proposed, inspired by the unique behaviors of end-functionalized homopolymers with attractive interaction where chain ends are associated, like branched polymers [112,113]. In comparison with the van der Waals interaction or hydrogen bonding, strong binding energy from covalently bonds in branched polymers are expected to lock the mobile chain ends tightly to fill the volume in nodes of network

phases. Various reports have demonstrated the synthetic routes for such polymers [114–117]. To simplify the controlling factors, star-BCPs with equal arm lengths are selected as the representatives.

A three-arm star-block (PS-*b*-PDMS)₃ was synthesized from the diblock precursor PS-*b*-PDMS ($M_n^{\text{PS}} = 12800$ g/mole, $M_n^{\text{PDMS}} = 10300$ g/mole, $D_M = 1.05$, $f_{\text{PDMS}}^v \sim 0.46$) with nearly symmetric composition for the study of the topology effect. The intrinsic phase (equilibrium phase) of both the diblock and star-block can be acquired by using a neutral solvent (cyclohexane). Projection with alternating dark and bright stripes under TEM can be observed [Fig. 15(a)], consistent with the calculated dimension in the SAXS profile [black lines in Figs. 15(d) and 15(e)], revealing the formation of the lamellae phase. No transition of phases can be found as the arm number increases except for the d spacing of the lamellae phases in the diblock and star-block. The phase transitions occur when the PS-selective solvent is utilized. For the diblock, the iconic wagon-wheel projection of a DG phase can be identified when a strongly PS-selective solvent, chlorobenzene, is used. The corresponding scattering profile also validates the

formation of a DG phase at which reflections labeled by the short black rods fit the theoretical prediction of a DG phase. Two additional peaks marked by the red rods can be also spotted, stating the possible nonaffine distortion of the structure owing to evaporation of the solvent [118,119]. In contrast, the windows for the DG phase through controlled self-assembly can be expanded in the star-block. The DG phase can be acquired by using a moderately PS-selective solvent such as chloroform and dichloromethane (DCM) for controlled self-assembly [Fig. 15(b)]. Furthermore, a phase transition occurs again as the selectivity of the solvent to the BCP intensifies. The projection of cylindrical morphology is taken under TEM, and reflections at the relative q values of $1:\sqrt{3}:2:\sqrt{7}:3:4$ [Fig. 15(e)] suggest the order-order transition to the hexagonally packed cylinder phase. The apparent difference between the final phase behaviors from the mix-and-match of solvents and the BCPs implicitly suggests the topology of BCP may provide a wider window for the aimed self-assembly. With the covalently bonded junctions, there will be intrinsic geometric asymmetry to the star-blocks due to the preference of bridging instead of bending conformations in self-assembled phases [117,120,121]. Consequently, the star-shaped junctions can be pinned in the center of the nodes, relieving the stretching stress to maintain the extended polymer chains in the central regions to avoid the formation of voids in the nodes and solve the packing frustration to the metastable network phases. In contrast, for the diblock, the flat PS-PDMS interfaces in the self-assembled structures can be found by using the moderately PS-selective solvent (chloroform and DCM), reflecting the extinction of the curving microdomains as the solvent evaporates. The low segregation strength of the diblock resulting from the low molecular weight might be insufficient to promote the extension of a polymer against the interface to the core of the nodes; the entropic penalty to packing frustration thus prevents formation of a DG phase. Furthermore, owing to the low molecular weight, the kinetics of highly stretched chains swollen by a solvent might be possible to rapidly resume their original dispositions before the vitrification. Eventually, the elastically stretched strings prefer to recover to their initial shape, resulting in the collapse of the metastable phases when phase transformation occurs. Those behaviors further demonstrate the characters of controlled self-assembly to acquire the metastable network phases at which the central theme is to acquire the aimed metastable phases from the equilibrium phases with the participation of a solvent to a kinetically trapped phase via order-order transitions.

VI. BIOMIMICKING NATURE FOR APPLICATIONS

In general, nanonetwork structures feature in providing a well-ordered continuous texture with a self-supporting framework, high surface area, and porosity in a nanometer length scale. Biomimicking from nature, organic and/or inorganic nanonetworks can be synthetically fabricated, giving broadness and effectiveness when tuning the desired properties [122–127]. Nanonetwork materials will be appealing in applications as metamaterials—materials whose effective properties do not result from the bulk behavior of the constituent materials but rather mainly from their de-

liberate structuring [128]. The Weyl materials can be an example to illustrate the concept [124,129,130]. By taking advantage of the TPMSs, degeneracies in a band structure mainly appear at highly symmetric points and stem from the existence of additional symmetries (beyond translation invariance) [124,129]. The photonic crystals are one of the categories of Weyl materials. Inspired by butterfly wings in nature, the bottom-up approach by self-assembly of BCPs can serve as a paradigmatic platform for constructing the nanostructures with TPMSs [123,131–133]. By taking advantage of the degradable BCP as a template, gyroid-structured organics and/or inorganics can be fabricated [134,135]. A facile templated synthesis approach has been proposed for the fabrication of nanomaterials with photonic optical responses by breaking the symmetry between two interpenetrating networks [131]. A natural translation of double networks can be achieved by melting the supporting polymeric matrix. Degradable BCPs can be used for preparation of the nanoporous template with a gyroid structure. Templated sol-gel reaction gives the replication of an inorganic SiO_2 nanonetwork within the polymer (PS) template [Fig. 16(a)] [122]. Owing to the difference between the thermal properties of the two materials, the polymer matrix will be molten before the inorganic networks. Consequently, the reallocation of networks erases the inversion center of the two coherent networks, resulting in shifted double networks with subgroup symmetry as compared with common DG [131]. It is thus to create a new reflection from the intrinsic DG at the relative q value of $\sqrt{2}$ that supports the transforming DG lattice. The new reflection is mostly observed in a SG phase (the same structure as the butterfly wings) or in a distorted DG lattice with nonaffine deformation [118,119]. Based on the reconstruction image from electron tomography, the additional reflection is indeed attributed to the shifting of the rigid property of SiO_2 networks [Fig. 16(e)]. The shifted DG SiO_2 networks with SG-like structural information are predicted to open a photonic band gap as a SG, exhibiting unique photonic behaviors [Figs. 16(b)–16(d)]. Similar strategies can be applied for fabrication of shifted DD networks through BCP templates obtained by controlled self-assembly by biomimicking the exoskeleton on beetles [Fig. 16(f)] [111].

Apart from the splendid colors that shine from the wing structures, the network structure within the bones gives superior strength to support the moving bodies with tens of sizes. The most outstanding network structure for mechanical performance was found in the dactyl club of a mantis shrimp [Fig. 17(a)] [24]. The hybrid cellular materials composed of hydroxyapatite (Hap) incorporated in an organic matrix show incredible impact resistance. The network texture of the nanohybrids contributes to the incredibility of the dactyl clubs. Bioinspired by the mantis shrimp, the fabrication of the well-ordered nanonetwork Hap can be achieved by using self-assembled PS-*b*-PDMS with a diamond structure from controlled self-assembly as a template for sol-gel reaction [Fig. 17(b)] [136]. Consequently, diamond-structured Hap can be successfully fabricated after removal of the polymeric template, giving nanoporous Hap with shifting of double networks [Fig. 17(c)], resulting in the pseudosingle-diamond structure with reflections at the relative q values of $\sqrt{3}:\sqrt{8}:\sqrt{11}:\sqrt{19}:\sqrt{27}$ [Fig. 17(d)]. The

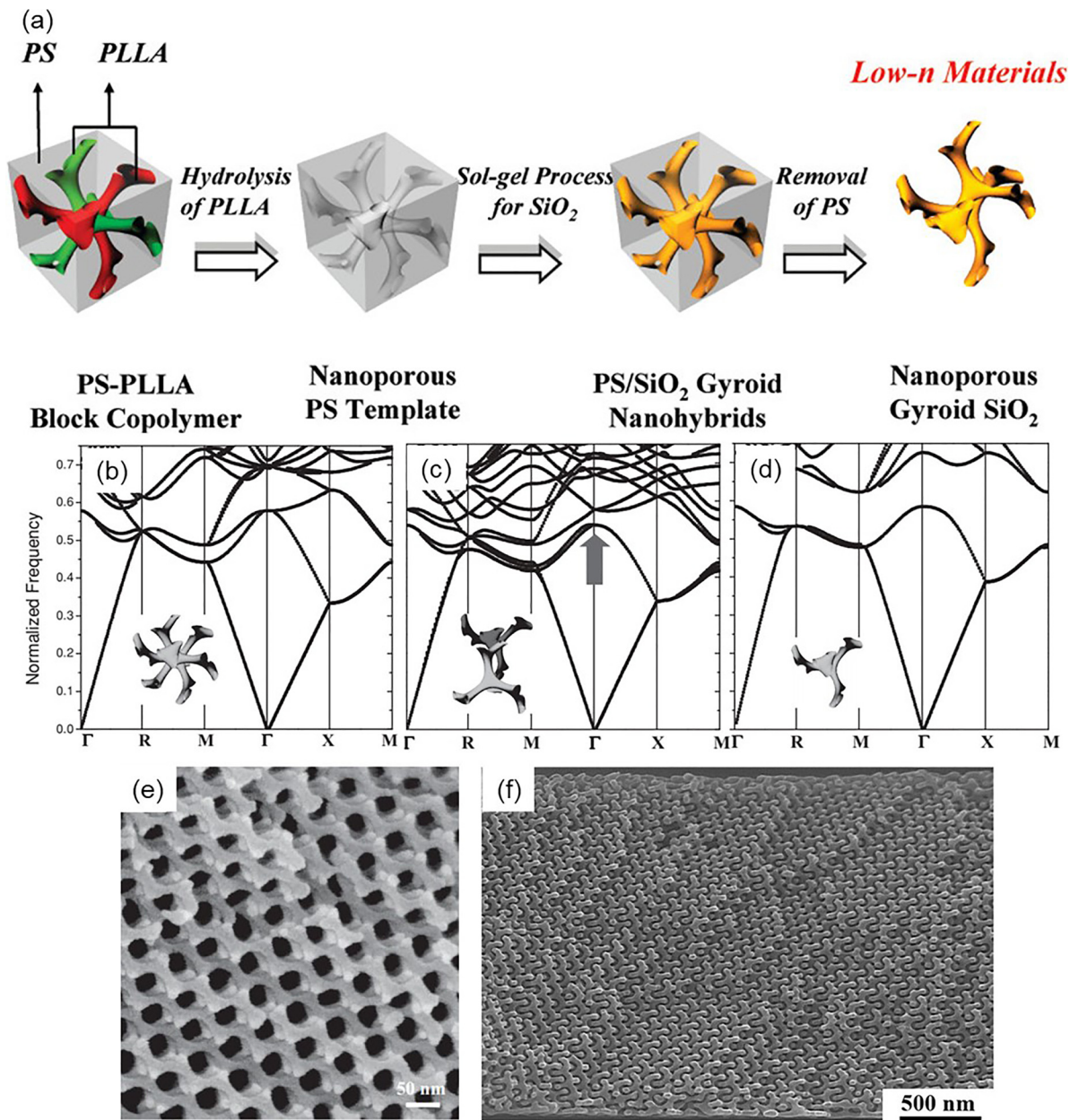


FIG. 16. (a) Schematic illustration for the creation of shifting ordered network from block copolymer (BCP) templated synthesis [122]. (b)–(d) Band structures of double gyroid (DG) network with various degrees of shifting [131]. Field-emission scanning electron microscopy (FESEM) micrograph of the fabricated SiO₂ nanonetworks with (e) shifted DG structure [131] and (f) shifted DD structure [111].

nanonetwork Hap monolith with a diamond texture can thus be successfully fabricated for mechanical analysis by using nanoindentation [136]. Based on the load-displacement curve from nanoindentation, the fabricated diamond-structured Hap shows a significant enhancement of the energy dissipation as indexed by the integration area of the close loop of the load-displacement curve [Fig. 17(f)] as compared with that of intrinsic Hap [Fig. 17(e)], giving the character of mechanical metamaterials. Moreover, the microcompression test shows that diamond-structured Hap exhibits a ductile character with large plastic deformation resulting from gradual layer-by-layer collapse instead of catastrophic failure for intrinsic Hap under compression; accordingly, the stress-strain curve of the nanonetwork Hap fabricated in contrast with intrinsic Hap

suggests a brittle-to-ductile transition due to the effect of deliberate structuring [137].

More cases of structures with TPMSs have also been discovered in the skeletons of knobby starfish *Protoreaster nodosus*, showing diamond contours which are considered a kind of network phase [138]. Unlike the functions of the exoskeleton in butterfly wings for shining splendid colors, the interior skeletons of starfish are used for support and protection of the soft organs and flesh in creature bodies. Materials with deliberate structuring as a network give superior mechanical performance far beyond the stochastic structure of their intrinsic components. Specifically, they deliver exquisite properties such as the negative Poisson's ratio, high stiffness, and specific energy absorption [139–142]. Sadek *et al.* [143]

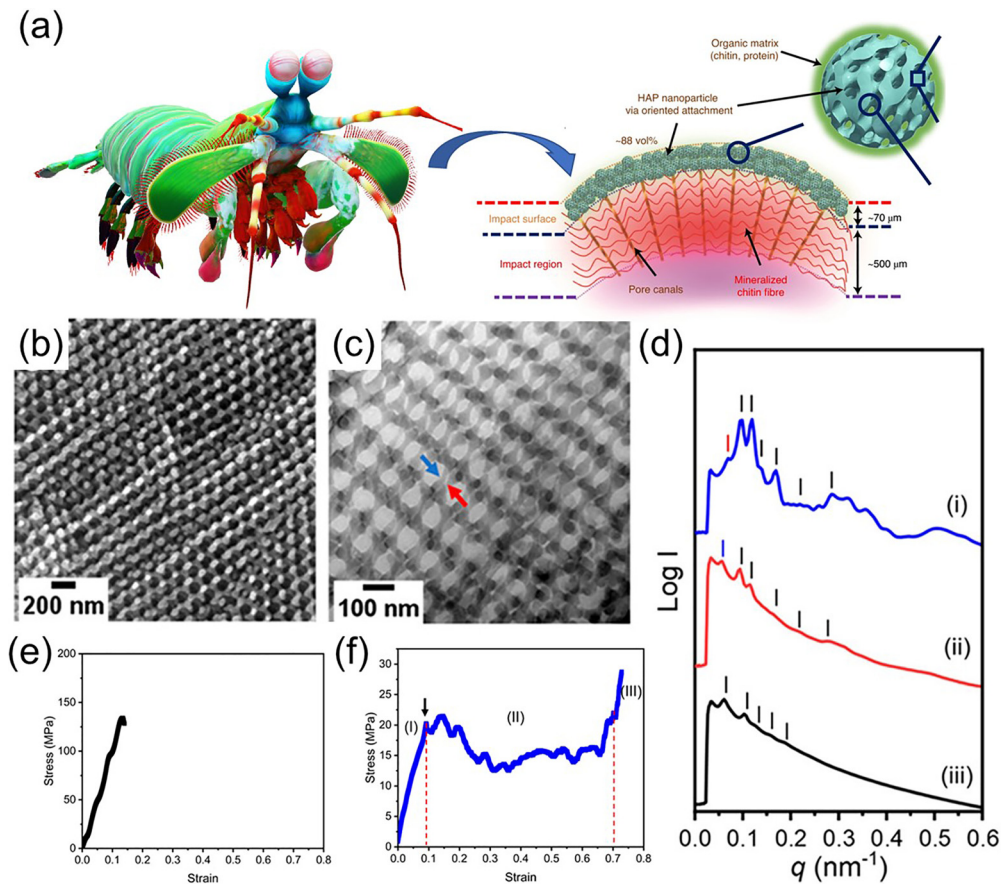


FIG. 17. (a) Schematic illustration of a mantis shrimp and its dactyl clubs with nanonetwork [24]. (b) Field-emission scanning electron microscopy (FESEM) micrographs of the templated sol-gel synthesis of nanonetwork hydroxyapatite (Hap) after removal of polystyrene (PS) template by thermal treatment. (c) Transmission electron microscopy (TEM) projections of the shifted double diamond (DD) networks. (d) One-dimensional (1D) small-angle x-ray scattering (SAXS) profiles of (i) nanoporous PS template obtained through controlled self-assembly of polystyrene-*block*-polydimethylsiloxane (PS-*b*-PDMS) followed by hydrofluoric acid (HF) etching, (ii) nanohybrids of PS/Hap and (iii) pseudosingle-diamond Hap from shifting of double networks [136].

demonstrated the feasibility of fabrication of nanonetwork materials with the same hierarchical structures yet at a smaller scale through templated crystallization synthesis of calcite single crystal (CSC). The diamond-structured template can be acquired by controlled self-assembly of PS-*b*-PDMS followed by hydrofluoric acid (HF) etching [135]. The fabricated diamond-structured CSC bears striking similarity to the skeleton of a knobby starfish, as shown in Fig. 18. Experimental and simulating results elucidate the process of deformation when compressing stress is applied to the structure. The appearance of the tetrapod can still be preserved after different loading stress which can be dissipated through the struts equally rather than concentrated at the nodes (Fig. 18); plastic deformation is endowed along the struts, preventing catastrophic fracture. Most significantly, the specialty of the diamond-structured calcite exhibits a large stress plateau with layer-by-layer collapse during compression, commencing smooth and noncatastrophic damage [137]. Moreover, in contrast with the starfish, a significantly high value of compressive strength can be obtained based on the stress-strain curve. Such a high performance exceeds various kinds of micro/nanolattice materials and even the natural CSC in knobby starfish due to the smaller feature size; that overcomes the

feature size limitation of fabrication from a top-down approach such as 3D printing and photolithography. Owing to the high strength and the large plastic deformation, the fabricated CSC bears a high capability for energy absorption, ~ 20 times of the starfish; that is indeed beyond nature for this artificial biomimicking well-ordered nanonetwork due to its smaller strut size. The effect of deliberating structure in mesoscale indeed outperforms the biomaterials, thoroughly reforming the brittle characteristic of CSC to ductilelike behavior with a higher degree of plastic transformation and thus incredible capacity for energy absorption. A bright future for biomimicking nanomaterials with network texture may be achieved for broad ranges of potential applications.

VII. CONCLUSIONS AND PERSPECTIVES

In this paper, we elucidate the recent progress from our group with respect to the investigation of the thermodynamic and kinetic factors of the controlled self-assembly of high- χ BCP, especially for PS-*b*-PDMS. In contrast with the conventional procedures for preparation of equilibrium phases in self-assembled BCPs, the usage of selective solvents and the kinetic control of the evaporation rate of solvents perturbs

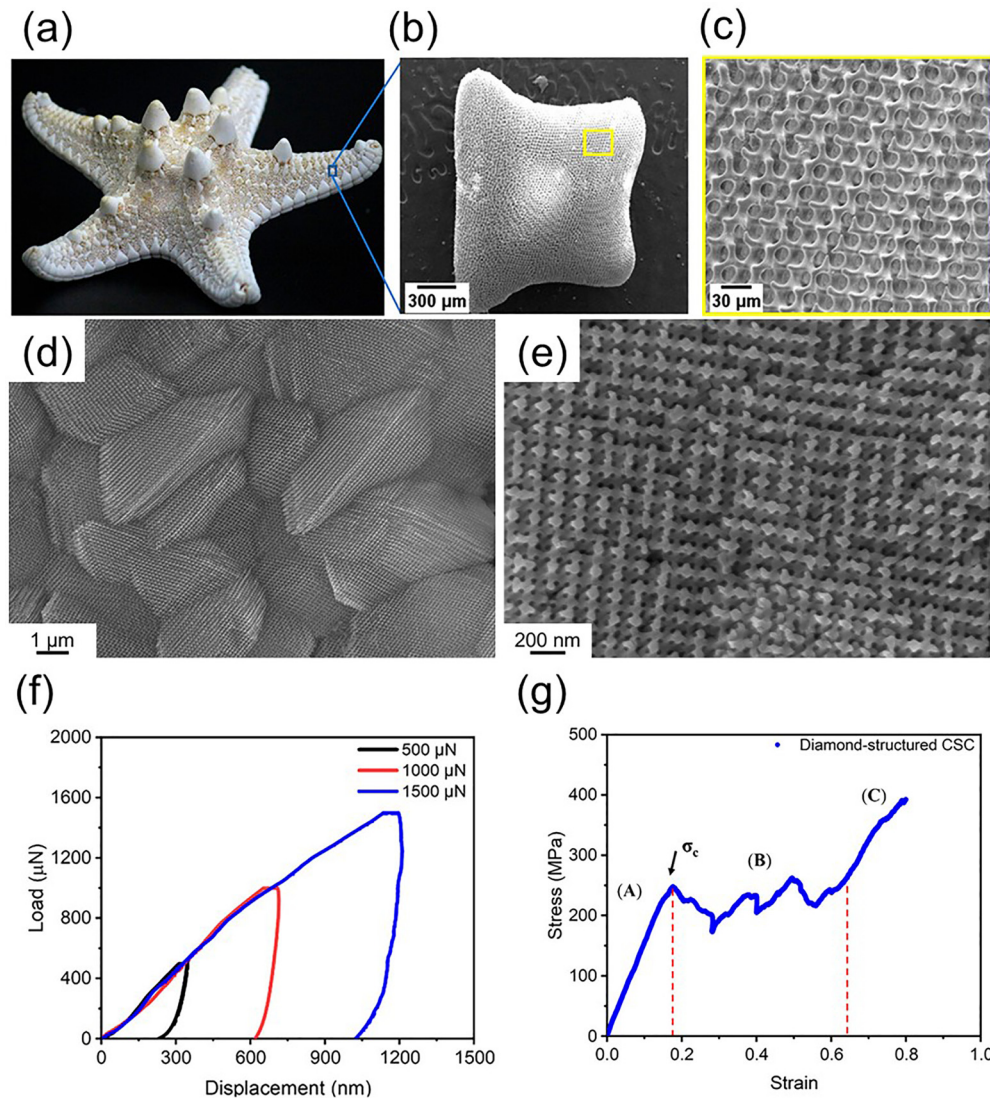


FIG. 18. The hierarchical structure of knobby starfish from (a) macroscopic overview. (b) Field-emission scanning electron microscopy (FESEM) micrograph of the surface of the ossicle in the skeleton. (c) Enlarged FESEM micrograph of the marked area in (b). (d) and (e) FESEM micrograph of diamond-structured calcite single crystal (CSC) fabricated by templated crystallization synthesis. (f) Load-displacement curves of the diamond-structured CSC by nanoindentation test. (g) Engineering stress-strain curve of the diamond-structured CSC measured by uniaxial microcompression [143].

stable environments, creating fluctuated conditions for kinetically capturing metastable phases; a variety of metastable phases with a high degree of ordering can be obtained from a single-composition lamellar phase. During the evaporation of the solvent, the different selectivities of the constituted blocks create asymmetry swelling that results in formation of curvatures corresponding to the final phase behaviors; a strongly selective solvent may create an inverted phase on the contrary. By taking advantage of such a facile approach, the DD phase with high packing frustration can be obtained as well as for the DP phase with the largest dimension of node sizes (i.e., highest entropic penalty). Moreover, the metastability of the forming network phases can be further investigated by temperature-resolved *in situ* SAXS experiments to decipher the origins of the complex phases. Most importantly, the concept of the combination of kinetics and thermodynamics for controlled self-assembly can be perfectly

transferred to the film state. Under different flow rates, the selective solvent will give completely different topologies of network phases. The DD phase can be obtained at a higher flow rate; the DG phase will be captured as the flow rate of the solvent reduces. Furthermore, the windows for network phases were even expanded through controlled self-assembly of star-BCPs as compared with the linear-conformation diblocks. The modification of conformations of BCPs could be another crucial factor to vary the phase behaviors that may give a variety of metastable network phases through a pathway by tuning the control factors of kinetics and thermodynamics.

Building on our earlier works on the platform technology of the templated synthesis of nanomaterials, metamaterials with outstanding functions can be achieved from the use of the acquired network phases. DG- and DD-structured SiO₂ and TiO₂ can be fabricated for examination of unique optical

properties. By taking advantage of the natural shifting of the forming double networks after removal of the polymeric template, the photonic band gap can be opened, showing similar optical properties to the butterfly wing structure. For applications to mechanical metamaterials, the extra struts of diamond as compared with the gyroid improve the energy dissipation as well as the impact resistance due to the averagely distributed stress along the struts with layer-by-layer collapse to avoid catastrophic failure on the framework. Such unusual mechanical behaviors originate from the structural design,

providing insights into engineering designs for metamaterials. Noticeably, there are still obstacles for the controlled self-assembly of high- χ BCPs such as the delicate synthesis of limited options for the components of BCPs and the precise control of the dynamic surroundings. Conclusively, the concept of controlled self-assembly of high- χ BCPs demonstrates the feasibility of achieving the unusual metastable network phases that can be used as templates for synthesis to create functional nanomaterials appealing to applications of multiple engineering fields.

-
- [1] F. S. Bates, Polymer-polymer phase behavior, *Science* **251**, 898 (1991).
- [2] F. S. Bates and G. H. Fredrickson, Block copolymers—Designer soft materials, *Phys. Today* **52**, 32 (1999).
- [3] F. S. Bates and G. H. Fredrickson, Block copolymer thermodynamics: Theory and experiment, *Annu. Rev. Phys. Chem.* **41**, 525 (1990).
- [4] Y. Mai and A. Eisenberg, Self-assembly of block copolymers, *Chem. Soc. Rev.* **41**, 5969 (2012).
- [5] E. E. Dormidontova and T. P. Lodge, The order-disorder transition and the disordered micelle regime in sphere-forming block copolymer melts, *Macromolecules* **34**, 9143 (2001).
- [6] G. M. Grason, Ordered phases of diblock copolymers in selective solvent, *J. Chem. Phys.* **126**, 114904 (2007).
- [7] H. Hückstädt, A. Göpfert, and V. Abetz, Synthesis and morphology of ABC heteroarm star terpolymers of polystyrene, polybutadiene and poly(2-vinylpyridine), *Macromol. Chem. Phys.* **201**, 296 (2000).
- [8] Y. Asai, K. Yamada, M. Yamada, A. Takano, and Y. Matsushita, Formation of tetragonally-packed rectangular cylinders from ABC block terpolymer blends, *ACS Macro Lett.* **3**, 166 (2014).
- [9] S. Foerster, A. K. Khandpur, J. Zhao, F. S. Bates, I. W. Hamley, A. J. Ryan, and W. Bras, Complex phase behavior of polyisoprene-polystyrene diblock copolymers near the order-disorder transition, *Macromolecules* **27**, 6922 (1994).
- [10] D. A. Hajduk, H. Takenouchi, M. A. Hillmyer, F. S. Bates, M. E. Vigild, and K. Almdal, Stability of the perforated layer (PL) phase in diblock copolymer melts, *Macromolecules* **30**, 3788 (1997).
- [11] V. Z.-H. Chan, J. Hoffman, V. Y. Lee, H. Iatrou, A. Avgeropoulos, N. Hadjichristidis, R. D. Miller, and E. L. Thomas, Ordered bicontinuous nanoporous and nanorelief ceramic films from self assembling polymer precursors, *Science* **286**, 1716 (1999).
- [12] T. S. Bailey, C. M. Hardy, T. H. Epps, and F. S. Bates, A noncubic triply periodic network morphology in poly(isoprene-*b*-styrene-*b*-ethylene oxide) triblock copolymers, *Macromolecules* **35**, 7007 (2002).
- [13] T. H. Epps, E. W. Cochran, T. S. Bailey, R. S. Waletzko, C. M. Hardy, and F. S. Bates, Ordered network phases in linear poly(isoprene-*b*-styrene-*b*-ethylene oxide) triblock copolymers, *Macromolecules* **37**, 8325 (2004).
- [14] T. H. Epps, E. W. Cochran, C. M. Hardy, T. S. Bailey, R. S. Waletzko, and F. S. Bates, Network phases in ABC triblock copolymers, *Macromolecules* **37**, 7085 (2004).
- [15] M. Takenaka, T. Wakada, S. Akasaka, S. Nishitsuji, K. Saijo, H. Shimizu, M. I. Kim, and H. Hasegawa, Orthorhombic *fddd* network in diblock copolymer melts, *Macromolecules* **40**, 4399 (2007).
- [16] R.-M. Ho, Y.-W. Chiang, C.-K. Chen, H.-W. Wang, H. Hasegawa, S. Akasaka, E. L. Thomas, C. Burger, and B. S. Hsiao, Block copolymers with a twist, *J. Am. Chem. Soc.* **131**, 18533 (2009).
- [17] X.-B. Wang, T.-Y. Lo, H.-Y. Hsueh, and R.-M. Ho, Double and single network phases in polystyrene-*block*-poly(l-lactide) diblock copolymers, *Macromolecules* **46**, 2997 (2013).
- [18] H.-F. Wang, P.-T. Chiu, C.-Y. Yang, Z.-H. Xie, Y.-C. Hung, J.-Y. Lee, J.-C. Tsai, I. Prasad, H. Jinnai, E. L. Thomas *et al.*, Networks with controlled chirality via self-assembly of chiral triblock terpolymers, *Sci. Adv.* **6**, eabc3644 (2020).
- [19] R.-M. Ho, Y.-W. Chiang, C.-C. Tsai, C.-C. Lin, B.-T. Ko, and B.-H. Huang, Three-dimensionally packed nanohelical phase in chiral block copolymers, *J. Am. Chem. Soc.* **126**, 2704 (2004).
- [20] J. W. Galusha, L. R. Richey, J. S. Gardner, J. N. Cha, and M. H. Bartl, Discovery of a diamond-based photonic crystal structure in beetle scales, *Phys. Rev. E* **77**, 050904(R) (2008).
- [21] V. Saranathan, C. O. Osuji, S. G. J. Mochrie, H. Noh, S. Narayanan, A. Sandy, E. R. Dufresne, and R. O. Prum, Structure, function, and self-assembly of single network gyroid ($I4_132$) photonic crystals in butterfly wing scales, *Proc. Natl. Acad. Sci. USA* **107**, 11676 (2010).
- [22] V. Saranathan, S. Narayanan, A. Sandy, E. R. Dufresne, and R. O. Prum, Evolution of single gyroid photonic crystals in bird feathers, *Proc. Natl. Acad. Sci. USA* **118**, e2101357118 (2021).
- [23] M. A. Meyers, J. McKittrick, and P.-Y. Chen, Structural Biological materials: Critical mechanics-materials connections, *Science* **339**, 773 (2013).
- [24] W. Huang, M. Shishebor, N. Guarín-Zapata, N. D. Kirchofer, J. Li, L. Cruz, T. Wang, S. Bhowmick, D. Stauffer, P. Manimunda *et al.*, A natural impact-resistant bicontinuous composite nanoparticle coating, *Nat. Mater.* **19**, 1236 (2020).
- [25] V. Saranathan, A. E. Seago, A. Sandy, S. Narayanan, S. G. J. Mochrie, E. R. Dufresne, H. Cao, C. O. Osuji, and R. O. Prum, Structural diversity of arthropod biophotonic nanostructures spans amphiphilic phase-space, *Nano Lett.* **15**, 3735 (2015).
- [26] E. L. Thomas, D. B. Alward, D. J. Kinning, D. C. Martin, D. L. Handlin, Jr., and L. J. Fetters, Ordered bicontinuous double-diamond structure of star block copolymers: A new equilibrium microdomain morphology, *Macromolecules* **19**, 2197 (1986).

- [27] Y. Mogi, H. Kotsuji, Y. Kaneko, K. Mori, and Y. Matsushita, Noda, I. Preparation and morphology of triblock copolymers of the ABC type, *Macromolecules* **25**, 5408 (1992).
- [28] A. H. Schoen, Infinite periodic minimal surfaces without self-intersections (NASA, Washington, D.C., 1970).
- [29] K. Grosse-Brauckmann, Triply periodic minimal and constant mean curvature surfaces, *Interface Focus* **2**, 582 (2012).
- [30] M. Nespolo, in *International Tables for Crystallography, Volume A, Space-Group Symmetry*, 6th ed., edited by M. I. Aroyo (Wiley, Hoboken, 2016).
- [31] M. Saba, M. D. Turner, K. Mecke, M. Gu, and G. E. Schröder-Turk, Group theory of circular-polarization effects in chiral photonic crystals with four-fold rotation axes applied to the eight-fold intergrowth of gyroid nets, *Phys. Rev. B* **88**, 245116 (2013).
- [32] I. Prasad, H. Jinnai, R.-M. Ho, E. L. Thomas, and G. M. Grason, Anatomy of triply-periodic network assemblies: Characterizing skeletal and inter-domain surface geometry of block copolymer gyroids, *Soft Matter* **14**, 3612 (2018).
- [33] M. W. Matsen and F. S. Bates, Unifying weak- and strong-segregation block copolymer theories, *Macromolecules* **29**, 1091 (1996).
- [34] M. W. Matsen and F. S. Bates, Block copolymer microstructures in the intermediate-segregation regime, *J. Chem. Phys.* **106**, 2436 (1997).
- [35] S. J. Park, G. K. Cheong, F. S. Bates, and K. D. Dorfman, Stability of the double gyroid phase in bottlebrush diblock copolymer melts, *Macromolecules* **54**, 9063 (2021).
- [36] S. P. Gido, D. W. Schwark, E. L. Thomas, and M. do Carmo Goncalves, Observation of a non-constant mean curvature interface in an ABC triblock copolymer, *Macromolecules* **26**, 2636 (1993).
- [37] M. W. Matsen and F. S. Bates, Origins of complex self-assembly in block copolymers, *Macromolecules* **29**, 7641 (1996).
- [38] T. Wen, H.-F. Wang, M.-C. Li, and R.-M. Ho, Homochiral Evolution in self-assembled chiral polymers and block copolymers, *Acc. Chem. Res.* **50**, 1011 (2017).
- [39] H.-F. Wang, K.-C. Yang, W.-C. Hsu, J.-Y. Lee, J.-T. Hsu, G. M. Grason, E. L. Thomas, J.-C. Tsai, and R.-M. Ho, Generalizing the effects of chirality on block copolymer assembly, *Proc. Natl. Acad. Sci. USA* **116**, 4080 (2019).
- [40] K.-C. Yang, A. Reddy, H.-W. Tsai, W. Zhao, G. M. Grason, and R.-M. Ho, Breaking mirror symmetry of double gyroids via self-assembly of chiral block copolymers, *ACS Macro Lett.* **11**, 930 (2022).
- [41] M.-C. Li, N. Ousaka, H.-F. Wang, E. Yashima, and R.-M. Ho, Chirality control and its memory at microphase-separated interface of self-assembled chiral block copolymers for nanostructured chiral materials, *ACS Macro Lett.* **6**, 980 (2017).
- [42] H.-F. Wang, L.-H. Yu, X.-B. Wang, and R.-M. Ho, A facile method to fabricate double gyroid as a polymer template for nanohybrids, *Macromolecules* **47**, 7993 (2014).
- [43] C.-Y. Chu, W.-F. Lin, J.-C. Tsai, C.-S. Lai, S.-C. Lo, H.-L. Chen, and T. Hashimoto, Order-order transition between equilibrium ordered bicontinuous nanostructures of double diamond and double gyroid in stereoregular block copolymer, *Macromolecules* **45**, 2471 (2012).
- [44] C.-H. Lin, T. Higuchi, H.-L. Chen, J.-C. Tsai, H. Jinnai, and T. Hashimoto, Stabilizing the ordered bicontinuous double diamond structure of diblock copolymer by configurational regularity, *Macromolecules* **51**, 4049 (2018).
- [45] H. A. Schwarz, *Gesammelte mathematische Abhandlungen* (Chelsea Pub. Co., New York, 1972).
- [46] M. W. Matsen, Stabilizing new morphologies by blending homopolymer with block copolymer, *Phys. Rev. Lett.* **74**, 4225 (1995).
- [47] F. J. Martínez-Veracoechea and F. A. Escobedo, Monte Carlo study of the stabilization of complex bicontinuous phases in diblock copolymer systems, *Macromolecules* **40**, 7354 (2007).
- [48] F. J. Martínez-Veracoechea and F. A. Escobedo, The plumber's nightmare phase in diblock copolymer/homopolymer blends. A self-consistent field theory study, *Macromolecules* **42**, 9058 (2009).
- [49] A. C. Finnefrock, R. Ulrich, A. Du Chesne, C. C. Honeker, K. Schumacher, K. K. Unger, S. M. Gruner, and U. Wiesner, Metal oxide containing mesoporous silica with bicontinuous "plumber's nightmare" morphology from a block copolymer-hybrid mesophase, *Angew. Chem. Int. Ed.* **40**, 1207 (2001).
- [50] L. Han, D. Xu, Y. Liu, T. Ohsuna, Y. Yao, C. Jiang, Y. Mai, Y. Cao, Y. Duan, and S. Che, Synthesis and characterization of macroporous photonic structure that consists of azimuthally shifted double-diamond silica frameworks, *Chem. Mater.* **26**, 7020 (2014).
- [51] Z. Guo, G. Zhang, F. Qiu, H. Zhang, Y. Yang, and A.-C. Shi, Discovering ordered phases of block copolymers: New results from a generic Fourier-space approach, *Phys. Rev. Lett.* **101**, 028301 (2008).
- [52] P.-T. Chiu, Y.-C. Sung, K.-C. Yang, J.-C. Tsai, H.-F. Wang, and R.-M. Ho, Curving and twisting in self-assembly of triblock terpolymers driven by a chiral end block, *Macromolecules* **55**, 1185 (2022).
- [53] P. Chen, F. S. Bates, and K. D. Dorfman, Alternating gyroid stabilized by surfactant-like triblock terpolymers in IS/SO/ISO ternary blends, *Macromolecules* **56**, 2568 (2023).
- [54] S. J. Park, F. S. Bates, and K. D. Dorfman, Complex phase behavior in binary blends of AB diblock copolymer and ABC triblock terpolymer, *Macromolecules* **56**, 1278 (2023).
- [55] Y. Asai, J. Suzuki, Y. Aoyama, H. Nishioka, A. Takano, and Y. Matsushita, Tricontinuous double diamond network structure from binary blends of ABC triblock terpolymers, *Macromolecules* **50**, 5402 (2017).
- [56] W. Takagi, J. Suzuki, Y. Aoyama, T. Mihira, A. Takano, and Y. Matsushita, Bicontinuous double-diamond structures formed in ternary blends of AB diblock copolymers with block chains of different lengths, *Macromolecules* **52**, 6633 (2019).
- [57] S. T. Hyde and F. C. Meldrum, Starfish grow extraordinary crystals, *Science* **375**, 615 (2022).
- [58] W. Mao, X. Cao, Q. Sheng, L. Han, and S. Che, Silica scaffold with shifted "plumber's nightmare" networks and their inter-conversion into diamond networks, *Angew. Chem.* **129**, 10810 (2017).
- [59] J.-F. Sadoc and J. Charvolin, Infinite periodic minimal surfaces and their crystallography in the hyperbolic plane, *Acta Cryst. A* **45**, 10 (1989).
- [60] A. M. Squires, R. H. Templer, J. M. Seddon, J. Woenkhaus, R. Winter, T. Narayanan, and S. Finet, Kinetics and mech-

- anism of the interconversion of inverse bicontinuous cubic mesophases, *Phys. Rev. E* **72**, 011502 (2005).
- [61] X. Zeng, G. Ungar, and M. Impéror-Clerc, A triple-network tricrystalline cubiquid crystal, *Nat. Mater.* **4**, 562 (2005).
- [62] C. Tschierske, Development of structural complexity by liquid-crystal self-assembly, *Angew. Chem. Int. Ed.* **52**, 8828 (2013).
- [63] W. Mao, X. Cao, Q. Sheng, L. Han, and S. Che, Silica scaffold with shifted “plumber’s nightmare” networks and their interconversion into diamond networks, *Angew. Chem. Int. Ed.* **56**, 10670 (2017).
- [64] S. Lidin, S. T. Hyde, and B. W. Ninham, Exact construction of periodic minimal-surfaces: The I-WP surface and its isometries, *J. Phys. France* **51**, 801 (1990).
- [65] Y. Kobayashi, R. Ohnuki, and S. Yoshioka, Discovery of I-WP minimal-surface-based photonic crystal in the scale of a longhorn beetle, *J. R. Soc., Interface* **18**, 20210505 (2021).
- [66] J. Zhao, B. Majumdar, M. F. Schulz, F. S. Bates, K. Almdal, K. Mortensen, D. A. Hajduk, and S. M. Gruner, Phase behavior of pure diblocks and binary diblock blends of poly (ethylene)-poly (ethylene), *Macromolecules* **29**, 1204 (1996).
- [67] C. A. Tyler and D. C. Morse, Orthorhombic *fddd* network in triblock and diblock copolymer melts, *Phys. Rev. Lett.* **94**, 208302 (2005).
- [68] F. S. Bates, M. F. Schulz, A. K. Khandpur, S. Förster, J. H. Rosedale, K. Almdal, and K. Mortensen, Fluctuations, conformational asymmetry and block copolymer phase behaviour, *Faraday Discuss.* **98**, 7 (1994).
- [69] H. Tanaka, H. Hasegawa, and T. Hashimoto, Ordered structure in mixtures of a block copolymer and homopolymers. 1. Solubilization of low molecular weight homopolymers, *Macromolecules* **24**, 240 (1991).
- [70] T. Hashimoto, S. Koizumi, and H. Hasegawa, Interfaces in block copolymer/homopolymer mixtures forming dry brushes, *Physica B* **213**, 676 (1995).
- [71] F. Chen, Y. Kondo, and T. Hashimoto, Control of nanostructure in mixtures of block copolymers: Curvature control via cosurfactant effects, *Macromolecules* **40**, 3714 (2007).
- [72] M. W. Bates, J. Lequeieu, S. M. Barbon, R. M. Lewis, III, K. T. Delaney, A. Anastasaki, C. J. Hawker, G. H. Fredrickson, and C. M. Bates, Stability of the A15 phase in diblock copolymer melts, *Proc. Natl. Acad. Sci. USA* **116**, 13194 (2019).
- [73] K. I. Winey, E. L. Thomas, and L. J. Fetters, The ordered bicontinuous double-diamond morphology in diblock copolymer/homopolymer blends, *Macromolecules* **25**, 422 (1992).
- [74] K. I. Winey, E. L. Thomas, and L. J. Fetters, Ordered morphologies in binary blends of diblock copolymer and homopolymer and characterization of their intermaterial dividing surfaces, *J. Chem. Phys.* **95**, 9367 (1991).
- [75] F. Court and T. Hashimoto, Morphological studies of binary mixtures of block copolymers. 1. Cosurfactant effects and composition dependence of morphology, *Macromolecules* **34**, 2536 (2001).
- [76] S. Ahn, J. Kwak, C. Choi, Y. Seo, J. K. Kim, and B. Lee, Gyroid structures at highly asymmetric volume fractions by blending of ABC triblock terpolymer and AB diblock copolymer, *Macromolecules* **50**, 9008 (2017).
- [77] F. S. Bates, M. A. Hillmyer, T. P. Lodge, C. M. Bates, K. T. Delaney, and G. H. Fredrickson, Multiblock polymers: Panacea or Pandora’s box? *Science* **336**, 434 (2012).
- [78] J. Park and K. I. Winey, Double gyroid morphologies in precise ion-containing multiblock copolymers synthesized via step-growth polymerization, *JACS Au* **2**, 1769 (2022).
- [79] G. Jo, H. Ahn, and M. J. Park, Simple route for tuning the morphology and conductivity of polymer electrolytes: One end functional group is enough, *ACS Macro Lett.* **2**, 990 (2013).
- [80] J. Paturej, S. S. Sheiko, S. Panyukov, and M. Rubinstein, Molecular structure of bottlebrush polymers in melts, *Sci. Adv.* **2**, e1601478 (2016).
- [81] B. R. Sveinbjörnsson, R. A. Weitekamp, G. M. Miyake, Y. Xia, H. A. Atwater, and R. H. Grubbs, Rapid self-assembly of brush block copolymers to photonic crystals, *Proc. Natl. Acad. Sci. USA* **109**, 14332 (2012).
- [82] J. Rzayev, Synthesis of polystyrene-poly lactide bottlebrush block copolymers and their melt self-assembly into large domain nanostructures, *Macromolecules* **42**, 2135 (2009).
- [83] L. Liberman, M. L. Coughlin, S. Weigand, F. S. Bates, and T. P. Lodge, Phase behavior of linear-bottlebrush block polymers, *Macromolecules* **55**, 2821 (2022).
- [84] R. Liang, Y. Xue, X. Fu, A. N. Le, Q. Song, Y. Qiang, Q. Xie, R. Dong, Z. Sun, and C. O. Osuji, Hierarchically engineered nanostructures from compositionally anisotropic molecular building blocks, *Nat. Mater.* **21**, 1434 (2022).
- [85] M. Seo and M. A. Hillmyer, Reticulated nanoporous polymers by controlled polymerization-induced microphase separation, *Science* **336**, 1422 (2012).
- [86] K. Kanamori, K. Nakanishi, and T. Hanada, Rigid macroporous poly (divinylbenzene) monoliths with a well-defined bicontinuous morphology prepared by living radical polymerization, *Adv. Mater.* **18**, 2407 (2006).
- [87] K. Yamamoto, E. Ito, S. Fukaya, and H. Takagi, Phase-separated conetwork structure induced by radical copolymerization of poly(dimethylsiloxane)- α,ω -diacrylate and *N,N*-dimethylacrylamide, *Macromolecules* **42**, 9561 (2009).
- [88] G. H. Fredrickson and K. Binder, Kinetics of metastable states in block copolymer melts, *J. Chem. Phys.* **91**, 7265 (1989).
- [89] X. Cheng, L. Lin, W. E. P. Zhang, and A.-C. Shi, Nucleation of ordered phases in block copolymers, *Phys. Rev. Lett.* **104**, 148301 (2010).
- [90] M. Müller and D.-W. Sun, Directing the self-assembly of block copolymers into a metastable complex network phase via a deep and rapid quench, *Phys. Rev. Lett.* **111**, 267801 (2013).
- [91] J. H. Rosedale, F. S. Bates, K. Almdal, K. Mortensen, and G. D. Wignall, Order and disorder in symmetric diblock copolymer melts, *Macromolecules* **28**, 1429 (1995).
- [92] P. J. Flory, Thermodynamics of high polymer solutions, *J. Chem. Phys.* **10**, 51 (1942).
- [93] M. A. Hillmyer, Nanoporous materials from block copolymer precursors, in *Block Copolymers II*, edited by V. Abetz (Springer, Berlin, 2005), pp. 137–181.
- [94] T. P. Lodge, X. Xu, C. Y. Ryu, I. W. Hamley, J. P. A. Fairclough, A. J. Ryan, and J. S. Pedersen, Structure and dynamics of concentrated solutions of asymmetric block copolymers in slightly selective solvents, *Macromolecules* **29**, 5955 (1996).

- [95] C.-I. Huang and T. P. Lodge, Self-consistent calculations of block copolymer solution phase behavior, *Macromolecules* **31**, 3556 (1998).
- [96] K. J. Hanley, T. P. Lodge, and C.-I. Huang, Phase behavior of a block copolymer in solvents of varying selectivity, *Macromolecules* **33**, 5918 (2000).
- [97] S. Hyde, S. Andersson, K. Larsson, Z. Blum, T. Landh, S. Lidin, and B. W. Ninham, *The Language of Shape: The Role of Curvature in Condensed Matter: Physics, Chemistry and Biology* (Elsevier, Amsterdam, 1997).
- [98] P. Sakya, J. M. Seddon, R. H. Templer, R. J. Mirkin, and G. J. T. Tiddy, Micellar cubic phases and their structural relationships: The nonionic surfactant system $C_{12}EO_{12}$ /water, *Langmuir* **13**, 3706 (1997).
- [99] T. Kaasgaard and C. J. Drummond, Ordered 2-D and 3-D nanostructured amphiphile self-assembly materials stable in excess solvent, *Phys. Chem. Chem. Phys.* **8**, 4957 (2006).
- [100] S. Ha, Y. La, and K. T. Kim, Polymer cubosomes: Infinite cubic mazes and possibilities, *Acc. Chem. Res.* **53**, 620 (2020).
- [101] T.-Y. Lo, C.-C. Chao, R.-M. Ho, P. Georgopoulos, A. Avgeropoulos, and E. L. Thomas, Phase transitions of polystyrene-*b*-poly(dimethylsiloxane) in solvents of varying selectivity, *Macromolecules* **46**, 7513 (2013).
- [102] L. H. Van Vlack, *Elements of Materials Science and Engineering* (Addison-Wesley Publishing Company, London, 1985).
- [103] P. G. de Gennes, *Scaling Concepts in Polymer Physics* (Cornell University Press, Ithaca, 1979).
- [104] M. Rubinstein and R. H. Colby, *Polymer Physics* (Oxford University Press, Oxford, 2003).
- [105] C.-Y. Chang, G.-M. Manesi, C.-Y. Yang, Y.-C. Hung, K.-C. Yang, P.-T. Chiu, A. Avgeropoulos, and R.-M. Ho, Mesoscale networks and corresponding transitions from self-assembly of block copolymers, *Proc. Natl. Acad. Sci. USA* **118**, e2022275118 (2021).
- [106] T. P. Lodge, B. Pudil, and K. J. Hanley, The full phase behavior for block copolymers in solvents of varying selectivity, *Macromolecules* **35**, 4707 (2002).
- [107] G. Kim and M. Libera, Morphological development in solvent-cast polystyrene-polybutadiene-polystyrene (SBS) triblock copolymer thin films, *Macromolecules* **31**, 2569 (1998).
- [108] Y. S. Jung and C. A. Ross, Orientation-controlled self-assembled nanolithography using a polystyrene-polydimethylsiloxane block copolymer, *Nano Lett.* **7**, 2046 (2007).
- [109] T. Hirai, M. Leolukman, C. C. Liu, E. Han, Y. J. Kim, Y. Ishida, T. Hayakawa, M.-a. Kakimoto, P. F. Nealey, and P. Gopalan, One-step direct-patterning template utilizing self-assembly of POSS-containing block copolymers, *Adv. Mater.* **21**, 4334 (2009).
- [110] J. N. L. Albert and T. H. Epps, Self-assembly of block copolymer thin films, *Mater. Today* **13**, 24 (2010).
- [111] T.-L. Lee, J.-W. Lin, and R.-M. Ho, Controlled self-assembly of polystyrene-*block*-polydimethylsiloxane for fabrication of nanonetwork silica monoliths, *ACS Appl. Mater. Interfaces* **14**, 54194 (2022).
- [112] A. N. Semenov, J. F. Joanny, and A. R. Khokhlov, Associating polymers: Equilibrium and linear viscoelasticity, *Macromolecules* **28**, 1066 (1995).
- [113] V. Schädler and U. Wiesner, Salt-controlled lamellar spacing in ionically end-capped symmetric diblock copolymers, *Macromolecules* **30**, 6698 (1997).
- [114] L.-K. Bi and L. J. Fetters, Synthesis and properties of block copolymers. 3. Polystyrene-polydiene star block copolymers, *Macromolecules* **9**, 732 (1976).
- [115] D. B. Alward, D. J. Kinning, E. L. Thomas, and L. J. Fetters, Effect of arm number and arm molecular weight on the solid-state morphology of poly(styrene-isoprene) star block copolymers, *Macromolecules* **19**, 215 (1986).
- [116] Y. Tselikas, H. Iatrou, N. Hadjichristidis, K. S. Liang, K. Mohanty, and D. J. Lohse, Morphology of miktoarm star block copolymers of styrene and isoprene, *J. Chem. Phys.* **105**, 2456 (1996).
- [117] P. Georgopoulos, T.-Y. Lo, R.-M. Ho, and A. Avgeropoulos, Synthesis, molecular characterization and self-assembly of (PS-*b*-PDMS)_{*n*} type linear (*n* = 1, 2) and star (*n* = 3, 4) block copolymers, *Polym. Chem.* **8**, 843 (2017).
- [118] X. Feng, C. J. Burke, M. Zhuo, H. Guo, K. Yang, A. Reddy, I. Prasad, R.-M. Ho, A. Avgeropoulos, G. M. Grason *et al.*, Seeing mesoatomic distortions in soft-matter crystals of a double-gyroid block copolymer, *Nature (London)* **575**, 175 (2019).
- [119] S. Jo, H. Park, T. Jun, K. Kim, H. Jung, S. Park, B. Lee, S. Lee, and D. Y. Ryu, Symmetry-breaking in double gyroid block copolymer films by non-affine distortion, *Appl. Mater. Today* **23**, 101006 (2021).
- [120] R. K. W. Spencer and M. W. Matsen, Domain bridging in thermoplastic elastomers of star block copolymer, *Macromolecules* **50**, 1681 (2017).
- [121] W. Jiang, Y. Qiang, W. Li, F. Qiu, and A.-C. Shi, Effects of chain topology on the self-assembly of AB-type block copolymers, *Macromolecules* **51**, 1529 (2018).
- [122] H.-Y. Hsueh, H.-Y. Chen, M.-S. She, C.-K. Chen, R.-M. Ho, S. Gwo, H. Hasegawa, and E. L. Thomas, Inorganic gyroid with exceptionally low refractive index from block copolymer templating, *Nano Lett.* **10**, 4994 (2010).
- [123] K. Hur, Y. Francescato, V. Giannini, S. A. Maier, R. G. Hennig, and U. Wiesner, Three-dimensionally isotropic negative refractive index materials from block copolymer self-assembled chiral gyroid networks, *Angew. Chem. Int. Ed.* **50**, 11985 (2011).
- [124] M. Fruchart, S.-Y. Jeon, K. Hur, V. Cheianov, U. Wiesner, and V. Vitelli, Soft self-assembly of Weyl materials for light and sound, *Proc. Natl. Acad. Sci. USA* **115**, E3655 (2018).
- [125] S. W. Robbins, P. A. Beaucage, H. Sai, K. W. Tan, J. G. Werner, J. P. Sethna, F. J. DiSalvo, S. M. Gruner, R. B. Van Dover, and U. Wiesner, Block copolymer self-assembly-directed synthesis of mesoporous gyroidal superconductors, *Sci. Adv.* **2**, e1501119 (2016).
- [126] L. Wang, J. Lau, E. L. Thomas, and M. C. Boyce, Continuous composite materials for stiffness, strength, and energy dissipation, *Adv. Mater.* **23**, 1524 (2011).
- [127] S. K. Siddique, T.-C. Lin, C.-Y. Chang, Y.-H. Chang, C.-C. Lee, S.-Y. Chang, P.-C. Tsai, Y.-R. Jeng, E. L. Thomas, and R.-M. Ho, Nanonetwork thermosets from templated polymerization for enhanced energy dissipation, *Nano Lett.* **21**, 3355 (2021).

- [128] N. Engheta and R. W. Ziolkowski, *Metamaterials: Physics and Engineering Explorations* (Wiley, Hoboken, 2006).
- [129] L. Lu, L. Fu, J. D. Joannopoulos, and M. Soljačić, Weyl points and line nodes in gyroid photonic crystals, *Nat. Photon.* **7**, 294 (2013).
- [130] B. Yan and C. Felser, Topological materials: Weyl semimetals, *Annu. Rev. Condens. Matter Phys.* **8**, 337 (2017).
- [131] H.-Y. Hsueh, Y.-C. Ling, H.-F. Wang, L.-Y. C. Chien, Y.-C. Hung, E. L. Thomas, and R.-M. Ho, Shifting networks to achieve subgroup symmetry properties, *Adv. Mater.* **26**, 3225 (2014).
- [132] S. Vignolini, N. A. Yufa, P. S. Cunha, S. Guldin, I. Rushkin, M. Stefik, K. Hur, U. Wiesner, J. J. Baumberg, and U. Steiner, A 3D optical metamaterial made by self-assembly, *Adv. Mater.* **24**, OP23 (2012).
- [133] M. D. Turner, M. Saba, Q. Zhang, B. P. Cumming, G. E. Schröder-Turk, and M. Gu, Miniature chiral beamsplitter based on gyroid photonic crystals, *Nat. Photon.* **7**, 801 (2013).
- [134] H.-Y. Hsueh, C.-T. Yao, and R.-M. Ho, Well-ordered nanohybrids and nanoporous materials from gyroid block copolymer templates, *Chem. Soc. Rev.* **44**, 1974 (2015).
- [135] T.-C. Lin, K.-C. Yang, P. Georgopoulos, A. Avgeropoulos, and R.-M. Ho, Gyroid-structured nanoporous polymer monolith from PDMS-containing block copolymers for templated synthesis, *Polymer* **126**, 360 (2017).
- [136] H. Sadek, S. K. Siddique, C. W. Wang, C. C. Lee, S. Y. Chang, and R. M. Ho, Bioinspired nanonetwork hydroxyapatite from block copolymer templated synthesis for mechanical metamaterials, *ACS Nano* **16**, 18298 (2022).
- [137] L. J. Gibson and M. F. Ashby, *Cellular Solids: Structure and Properties* (Cambridge University Press, Cambridge, 1997).
- [138] T. Yang, H. Chen, Z. Jia, Z. Deng, L. Chen, E. M. PETERMAN, J. C. Weaver, and L. Li, A damage-tolerant, dual-scale, single-crystalline microlattice in the knobby starfish, *Protoreaster nodosus*, *Science* **375**, 647 (2022).
- [139] J.-H. Lee, J. P. Singer, and E. L. Thomas, Micro-/nanostructured mechanical metamaterials, *Adv. Mater.* **24**, 4782 (2012).
- [140] Z. G. Nicolaou and A. E. Motter, Mechanical metamaterials with negative compressibility transitions, *Nat. Mater.* **11**, 608 (2012).
- [141] T. A. M. Hewage, K. L. Alderson, A. Alderson, and F. Scarpa, Double-negative mechanical metamaterials displaying simultaneous negative stiffness and negative Poisson's ratio properties, *Adv. Mater.* **28**, 10323 (2016).
- [142] T. Frenzel, M. Kadic, and M. Wegener, Three-dimensional mechanical metamaterials with a twist, *Science* **358**, 1072 (2017).
- [143] H. Sadek, S. K. Siddique, C. W. Wang, P. T. Chiu, C. C. Lee, and R. M. Ho, Starfish-inspired diamond-structured calcite single crystals from a bottom-up approach as mechanical metamaterials, *ACS Nano* **17**, 15678 (2023).